Real-Time Evolution of Open Quantum Spin Systems driven by Measurements

Master Thesis

at the Institute for Theoretical Physics, Science Faculty, University of Bern
by

Franziska Schranz

March, 2015

Supervisor:
Prof. Dr. Uwe-Jens Wiese
Institute for Theoretical Physics, University of Bern

Abstract

We study the real-time dynamics of different quantum spin 1/2 systems that are coupled to the environment by dissipative measurement processes. The system is defined on a 2-dimensional square lattice and its dynamics is entirely driven by measurements performed on neighboring spin pairs. The coupling to the environment is described by the Kossakowski-Lindblad equation. We present three different measurement processes and show that the sign problem is solved by summing over the intermediate measurement results. We derive the cluster-rules for these measurement processes in order to simulate the real-time evolution of the system with an efficient loop-cluster algorithm. The investigation of the real-time dynamics of the Fourier modes of the magnetization shows that the initially ordered states are driven to a new equilibrium. If the measurement process conserves one of the Fourier modes we observe a slower equilibration for the modes close to the conserved mode than for the other modes.

Contents

1 Introduction

The simulation of a quantum system far from equilibrium is a very challenging problem on a classical computer. On the one hand it is not possible to diagonalize the Hamiltonian for large quantum systems since the Hilbert space grows exponentially with the volume of the system. On the other hand the Monte Carlo importance sampling, that is a well established method to simulate quantum systems in thermal equilibrium, can not be used to simulate systems far from equilibrium since they suffer from a severe sign or complex weight problem.

An exception are gapped 1-dimensional systems with small entanglement for which the matrix product states are underlying the density matrix renormalization group [1, 2]. Such systems can be simulated in real time at least for moderate time intervals [3]. However it is not possible to simulate a general quantum system over a large real-time period on a classical computer.

A universal quantum simulator, which was proposed by Feynman already in 1982 [4], should be able to calculate this real-time evolution. In recent years there was major progress in the field of quantum optics. First devices of quantum simulators have been realized with ultra-cold atoms in optical lattices. However, these quantum simulators are far from being generally applicable. The calculation of the real-time evolution of quantum systems on classical computers is still an important problem to solve.

In nature quantum systems are usually coupled to an environment which makes them behave more classical. This should make it easier to calculate their evolution on a classical computer. The coupling to the environment is described by the Kossakowski-Lindblad equation [5, 6]. In this thesis we study the evolution of quantum spin systems that are coupled to an environment through dissipative measurement processes. For the moment we totally neglect the Hamiltonian and drive the system only by dissipative measurements on pairs of neighboring spins. By performing measurements on spin pairs the initially ordered states are driven to a new equilibrium. One possibility to drive the system forward in real time is to measure the total spin of two neighboring spins. The observed real-time dynamics of the Fourier modes of the magnetization depends on the symmetries of the measurement processes. The initial density matrices are built according to the anti-ferromagnetic Heisenberg model, the ferromagnetic Heisenberg model or the XY-model. We simulate this evolution with a loop-cluster algorithm in discrete time. However, we could also directly work in the Euclidean time continuum by using a continuous-time version of the loop cluster algorithm [7].

It is a challenge to understand the real time behavior of the anti-ferromagnet which was of such importance in physics that its fundamental description led to a Nobel Prize. Louis Néel received the Prize in 1970 for "fundamental work and discoveries concerning anti-ferromagnetism and ferrimagnetism which have led to important applications in solid state physics" [8].

The structure of this thesis is as follows. We give a brief introduction to the quantum spin system and the setting in section 2. In section 3 we describe how to simulate a quantum spin system in thermal equilibrium. We derive the path

integral formulation of the partition function which leads us to the formulation of the loop-cluster algorithm in Euclidean time. In section 4 we discuss a path integral expression for the measurement driven real-time evolution of the initial density matrix. We introduce three measurement processes that can be used to drive the evolution. If we neglect the Hamiltonian and sum over the intermediate measurement results we get rid of the sign and complex weight problem and are able to simulate the real-time evolution of a quantum spin system using a loop-cluster algorithm. Thereafter, in section 5, we discuss the dynamics of the Fourier modes of the magnetization driven by the three different measurement processes. The initial density matrix, where the evolution started from, is given by either the Heisenberg anti-ferromagnet, the Heisenberg ferromagnet or the XY-model at low temperature. We also analyze the equilibration times for the different measurement processes. In the appendix it is explained how the calculation of the error and the fit was performed using a Jackknife re-sampling of the data.

We will work in natural units where $\hbar = k_B = c = 1$.

2 Quantum Spin Systems

The quantum spin systems we will consider are described by the following Hamiltonian

$$\mathbb{H} = \sum_{\langle xy \rangle} J \left(S_x^1 S_y^1 + S_x^2 S_y^2 \right) + J' S_x^3 S_y^3 \,, \tag{2.1}$$

where x and y are the coordinates of lattice sites and $\langle xy \rangle$ denotes a pair of nearest neighbors. S_x^i, $i \in \{1,2,3\}$ are quantum spin $\frac{1}{2}$ operators at the site x. They are given by

$$\vec{S}_x = \frac{\hbar}{2} \left(\sigma_1, \sigma_2, \sigma_3 \right) \,, \tag{2.2}$$

where $\hbar = 1$ and σ_i are the Pauli matrices

$$\sigma_1 = \begin{pmatrix} 0 & 1 \\ 1 & 0 \end{pmatrix}, \quad \sigma_2 = \begin{pmatrix} 0 & i \\ -i & 0 \end{pmatrix}, \quad \sigma_3 = \begin{pmatrix} 1 & 0 \\ 0 & -1 \end{pmatrix}. \tag{2.3}$$

The quantum spin operators are the generators of an $SU(2)$ algebra

$$\left[S_x^a, S_y^b \right] = i \delta_{xy} \varepsilon^{abc} S_x^c. \tag{2.4}$$

Which specific model is described by the above Hamiltonian depends on the parameters J and J'. If $J = J' > 0$ we have a anti-ferromagnetic Heisenberg model. For $J = J' < 0$ it describes a ferromagnetic Heisenberg model and for $J' = 0$ it describes the XY-model. If $J = 0$ we have a classical Ising model which won't be considered any further.

2.1 Setting

We will perform numerical simulations on a $L \times L$ square lattice with periodic boundary conditions. The boundary conditions are chosen in this way in order to conserve translation invariance. Additionally the lattice needs to be bipartite which means that the lattice can be decomposed into two identical sub-lattices. Therefore the number of sites L has to be an even number. For a quantum spin system on a 2-dimensional $L \times L$ lattice the dimension of the Hilbert space is $\dim(\mathcal{H}) = 2^{L \times L}$.

The quantization direction chosen for the quantum spins will generally be the 3-direction. For some special cases we will turn to the 1-direction as the quantization axis.

The Hilbert space for a one-spin system quantized in the 3-direction contains the following states

$$\mathcal{H}_x = \{ |s_x\rangle \} = \{ |\uparrow\rangle, |\downarrow\rangle \}. \tag{2.5}$$

They are the eigenstates of the quantum spin operator S_x^3 with eigenvalues $\{+\frac{1}{2}, -\frac{1}{2}\}$.

A vector representation for these states is given by

$$|\uparrow\rangle = \begin{pmatrix} 1 \\ 0 \end{pmatrix}, \qquad |\downarrow\rangle = \begin{pmatrix} 0 \\ 1 \end{pmatrix}. \tag{2.6}$$

For a two-spin system with spins at the sites x and y the Hilbert space is the tensor product of the two individual Hilbert spaces

$$\mathcal{H} = \mathcal{H}_x \otimes \mathcal{H}_y = \{|s_x\rangle \otimes |s_y\rangle\} = \{|s_x s_y\rangle\} = \{|\uparrow\uparrow\rangle, |\uparrow\downarrow\rangle, |\downarrow\uparrow\rangle, |\downarrow\downarrow\rangle\}. \tag{2.7}$$

In the vector representation used above these states are expressed as

$$|\uparrow\uparrow\rangle = \begin{pmatrix} 1 \\ 0 \\ 0 \\ 0 \end{pmatrix}, \quad |\uparrow\downarrow\rangle = \begin{pmatrix} 0 \\ 1 \\ 0 \\ 0 \end{pmatrix}, \quad |\downarrow\uparrow\rangle = \begin{pmatrix} 0 \\ 0 \\ 1 \\ 0 \end{pmatrix}, \quad |\downarrow\downarrow\rangle = \begin{pmatrix} 0 \\ 0 \\ 0 \\ 1 \end{pmatrix}. \tag{2.8}$$

2.2 Partition function

To describe a system in thermal equilibrium one uses the partition function which is defined as

$$Z = \mathrm{Tr}(e^{-\beta \mathbb{H}}) \, . \tag{2.9}$$

With a known partition function it is possible to evaluate the expectation value of an observable represented by the operator $\mathcal{O}$

$$\langle \mathcal{O} \rangle = \frac{1}{Z} \mathrm{Tr}(\mathcal{O} e^{-\beta \mathbb{H}}). \tag{2.10}$$

When we introduce the definition of the density matrix

$$\rho = \frac{1}{Z} e^{-\beta \mathbb{H}} \, , \qquad \mathrm{Tr}(\rho) = 1 \, , \tag{2.11}$$

we are able to write

$$\langle \mathcal{O} \rangle = \mathrm{Tr}(\mathcal{O}\rho). \tag{2.12}$$

3 Derivation of the Path Integral and the Loop-Cluster Algorithm

We want to calculate the expectation value of an observable for a quantum spin system which is in equilibrium (canonical ensemble). We have seen in equation (2.10) that the expectation value of an observable can be expressed as

$$\langle \mathcal{O} \rangle = \frac{1}{Z} \operatorname{Tr}(\mathcal{O} e^{-\beta \mathbb{H}}). \tag{3.1}$$

For a large quantum spin system this quantity can not be evaluated analytically because the dimension of the Hilbert space is $\dim(\mathcal{H}) = 2^V$. This means that the dimension of the Hilbert space grows exponentially with the volume of the system and it therefore is not possible to diagonalize the Hamiltonian for large systems. Instead we will use a Monte Carlo simulation to calculate the expectation value.

In this section we will construct the loop cluster algorithm, which is a highly efficient Monte Carlo algorithm for quantum spin systems in equilibrium. Therefore we will first derive the path integral representation of the partition function. After a brief introduction into the subject of Monte Carlo simulations we will construct the loop algorithm for a one-dimensional spin chain. Afterwards we generalization this algorithm for a two-dimensional system. The spin model used in the beginning will then be replaced by a bond model which defines the rules of the loop cluster algorithm. This section is based on [9–11].

3.1 The Path Integral Representation of the Partition Function

For simplicity we derive the loop cluster algorithm for a 1-dimensional spin chain of length L_x described by the Hamiltonian $\mathbb{H}$. The generalization to higher dimensions is then straightforward. We will start with a path integral formulation of the partition function Z.

The Hamiltonian of this system can be divided into two parts.

$$\mathbb{H} = \mathbb{H}_1 + \mathbb{H}_2 \ , \tag{3.2}$$

where $\mathbb{H}_1$ sits at the even and $\mathbb{H}_2$ at the odd bonds as we show in Figure 1.

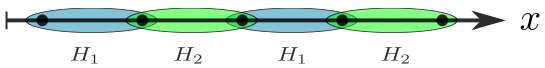

Figure 1: The Hamiltonian of the system is divided into two parts $\mathbb{H} = \mathbb{H}_1 + \mathbb{H}_2$. Each of the Hamiltonians acts on neighboring spins either connected by even or odd links.

The operators $\mathbb{H}_1$ and $\mathbb{H}_2$ are defined as

$$\mathbb{H}_1 = \sum_{x=2m} J\left(S_x^1 S_{x+1}^1 + S_x^2 S_{x+1}^2\right) + J' S_x^3 S_{x+1}^3 = \sum_{x=2m} \mathbb{h}_{x,x+1}, \quad (3.3)$$

$$\mathbb{H}_2 = \sum_{x=2m+1} J\left(S_x^1 S_{x+1}^1 + S_x^2 S_{x+1}^2\right) + J' S_x^3 S_{x+1}^3 = \sum_{x=2m+1} \mathbb{h}_{x,x+1}, \quad (3.4)$$

where $m \in \{0, ..., L_x - 1\}$ and $\mathbb{h}_{x,x+1}$ is called link Hamiltonian. It represents a two-spin interaction of a spin at site x and a spin at site $x+1$. Let us now introduce β, a and N. β is the Euclidean time which is proportional to the inverse temperature, a is the lattice spacing in euclidean time direction and N is the number of time slices given by $\beta = aN$. Hence the partition function can be written as

$$Z = \mathrm{Tr}(e^{-\beta \mathbb{H}}) = \lim_{N\to\infty} \mathrm{Tr}\left[\left(e^{-a(\mathbb{H}_1+\mathbb{H}_2)}\right)^N\right]. \quad (3.5)$$

For the second equality we used the Trotter decomposition formula

$$e^{A+B} = \lim_{N\to\infty} \left(e^{A/N} e^{B/N}\right)^N, \quad (3.6)$$

where A and B are non-commuting operators. By inserting complete sets of states $\sum_n |n\rangle \langle n| = \mathbb{1}$ one can write the partition function as a path integral

$$\begin{aligned} Z &= \lim_{a\to 0} \sum_{n_1, n_2, ..., n_{2N}} \langle n_{2N}| e^{-a\mathbb{H}_1} |n_1\rangle \langle n_1| e^{-a\mathbb{H}_2} |n_2\rangle \cdot \ ... \\ &\quad \cdot \langle n_{2N-1}| e^{-a\mathbb{H}_2} |n_{2N}\rangle \ . \end{aligned} \quad (3.7)$$

The state $|n\rangle$ denotes the spin configuration in one time slice of the lattice. When we take the limit $a \to 0$ we use that $aN = \beta$ is fixed so N goes to infinity simultaneously. One lattice spacing a contains two time steps $\Delta\tau$. In the first time step the Hamiltonian $\mathbb{H}_1$ is active and in the second $\mathbb{H}_2$ is active. This leads to a covering of the lattice by active and inactive plaquettes in a checkerboard pattern as we show in Figure 2.

The operator $e^{-a\mathbb{H}_1}$ evolves the current state of the spin chain one step forward in time. As we can see from equation (3.4), $\mathbb{H}_1$ is composed of link Hamiltonians $\mathbb{h}_{x,x+1}$ which commute with each other since they act on different links that have no intersection. The factors from equation (3.7) are therefore decomposed into

$$\begin{aligned} \langle n_i| e^{-a\mathbb{H}_1} |n_{i+1}\rangle &= \langle n_i| e^{-a\sum_{x=2m} \mathbb{h}_{x,x+1}} |n_{i+1}\rangle \\ &= \prod_{x=2m} \left\langle S^z_{x,t_i} S^z_{x+1,t_i}\right| e^{-a\mathbb{h}_{x,x+1}} \left| S^z_{x,t_{i+1}}, S^z_{x+1,t_{i+1}}\right\rangle \end{aligned} \quad (3.8)$$

where $i \in \{1, ..., 2N\}$. The object $S^z_{x,t}$ denotes the third component of the spin sitting at site (x,t). These link Hamiltonians evolve two neighboring spins

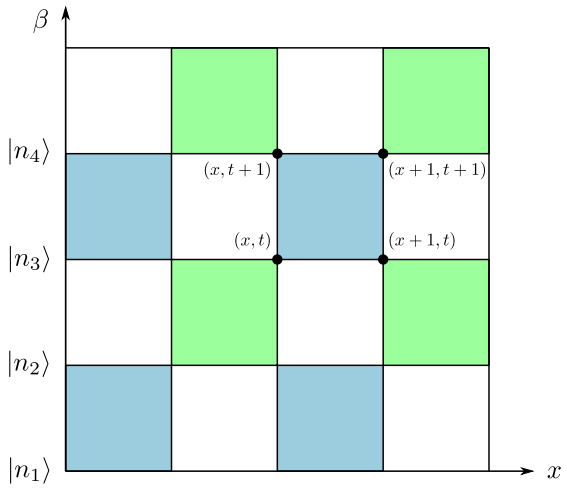

Figure 2: The Hamiltonian acts in a checkerboard pattern. In the first time-step $\mathbb{H}_1$ is active (blue) and in the second time-step $\mathbb{H}_2$ is active (green). These two time-steps are contained in one lattice spacing $a = \Delta\tau$. The four corners of a plaquette are indicated by $p = ((x,t),(x+1,t),(x,t+1),(x+1,t+1))$.

trough one time step. For the operator $\mathbb{H}_2$ this works analogously. The partition function is then written as a sum over all possible spin configurations $\mathcal{S} = \{S^z_{x,t}\}$ and a product over all plaquettes p. The limit from $a \to 0$ is neglected here.

$$\begin{aligned} Z &= \sum_{\{S^z_{x,t}\}} \prod_p \left\langle S^z_{x,t} S^z_{x+1,t} \right| e^{-a\mathbb{h}_{x,x+1}} \left| S^z_{x,t+1}, S^z_{x+1,t+1} \right\rangle \\ &= \sum_{\mathcal{S}} \prod_p W(\{S_p\}) \;=\; \sum_{\mathcal{S}} W(\mathcal{S})\,. \end{aligned} \tag{3.9}$$

Here S_p is the 4-tuple of spins located at the corners of a plaquette $p = ((x,t),(x+1,t),(x,t+1),(x+1,t+1))$ which is indicated in Figure 2. We now can go to one single plaquette and see which evolutions in euclidean time are allowed for two neighboring spins. Therefore we need to calculate the transfer matrix. We use the Hamiltonian given in equation (2.1).

$$T^z = e^{-a\mathbb{h}_{x,x+1}} = \begin{pmatrix} e^{-\frac{a}{4}J'} & 0 & 0 & 0 \\ 0 & e^{\frac{a}{4}J'}\cosh\left(\frac{a}{2}J\right) & -e^{\frac{a}{4}J'}\sinh\left(\frac{a}{2}J\right) & 0 \\ 0 & -e^{\frac{a}{4}J'}\sinh\left(\frac{a}{2}J\right) & e^{\frac{a}{4}J'}\cosh\left(\frac{a}{2}J\right) & 0 \\ 0 & 0 & 0 & e^{-\frac{a}{4}J'} \end{pmatrix}, \tag{3.10}$$

where $\mathbb{h}_{x,x+1}$ is given by

$$\mathbb{h}_{x,x+1} = J\left(S_x^1 S_y^1 + S_x^2 S_y^2\right) + J' S_x^3 S_y^3 = \frac{1}{4}\begin{pmatrix} J' & 0 & 0 & 0 \\ 0 & -J' & 2J & 0 \\ 0 & 2J & -J' & 0 \\ 0 & 0 & 0 & J' \end{pmatrix}. \tag{3.11}$$

This transfer matrix provides the allowed configurations on a plaquette and its weights

$$\begin{aligned} W(1^{\pm}) &= \langle\uparrow\uparrow|\, e^{-a\mathbb{h}_{x,x+1}}\, |\uparrow\uparrow\rangle = \langle\downarrow\downarrow|\, e^{-a\mathbb{h}_{x,x+1}}\, |\downarrow\downarrow\rangle = e^{-\frac{a}{4}J'}, \\ W(2^{\pm}) &= \langle\uparrow\downarrow|\, e^{-a\mathbb{h}_{x,x+1}}\, |\uparrow\downarrow\rangle = \langle\downarrow\uparrow|\, e^{-a\mathbb{h}_{x,x+1}}\, |\downarrow\uparrow\rangle = e^{\frac{a}{4}J'} \cosh\left(\frac{a}{2}J\right), \\ W(3^{\pm}) &= \langle\uparrow\downarrow|\, e^{-a\mathbb{h}_{x,x+1}}\, |\downarrow\uparrow\rangle = \langle\downarrow\uparrow|\, e^{-a\mathbb{h}_{x,x+1}}\, |\uparrow\downarrow\rangle = e^{\frac{a}{4}J'} \sinh\left(\frac{a}{2}|J|\right). \end{aligned} \tag{3.12}$$

Considering the transfer matrix the weight $W(3^{\pm})$ would actually be negative and cause a sign problem. Since the expectation value of an observable is independent of the chosen basis we can always perform a uniform transformation on the Hamiltonian to change the basis. Performing the staggered transformation

$$S_x^1 \to -S_x^1, \qquad S_x^2 \to -S_x^2, \qquad S_x^3 \to S_x^3, \tag{3.13}$$

on one of the two sub lattices of a bipartite lattice is the same as changing the sign of J. The matrix representation of this uniform transformation for a two spin system is

$$U = \begin{pmatrix} -1 & 0 \\ 0 & 1 \end{pmatrix} \otimes \mathbb{1} = \begin{pmatrix} -1 & 0 & 0 & 0 \\ 0 & -1 & 0 & 0 \\ 0 & 0 & 1 & 0 \\ 0 & 0 & 0 & 1 \end{pmatrix}. \tag{3.14}$$

This means that we always can choose J to be negative and thereby get rid of the minus sign in front of the hyperbolic sine. The weight $W(3^{\pm})$ is therefore always positive.

From this short calculation we know the allowed spin configurations on a plaquette and their weights. We need to construct an algorithm that updates a spin configuration on the lattice $\mathcal{S} \to \mathcal{S}'$ according to its weight distribution. Before we construct the loop-cluster algorithm we will give a short introduction into the subject of Monte Carlo simulations.

3.2 The Monte Carlo Procedure

With a Monte Carlo procedure one can calculate the expectation value of ab observable statistically. An expectation value of an operator $\langle\mathcal{O}\rangle$ is given by

$$\langle\mathcal{O}\rangle = \frac{1}{Z}\,\mathrm{Tr}(\mathcal{O}e^{-\beta\mathbb{H}}) = \frac{1}{Z}\sum_{\mathcal{S}} \mathcal{O}(\mathcal{S})W(\mathcal{S}). \tag{3.15}$$

Where $\mathcal{S}$ are all possible configurations of a system, $\mathcal{O}(\mathcal{S})$ denotes the value of the observable evaluated for a configuration $\mathcal{S}$ and $W(\mathcal{S})$ is the weight of the configuration $\mathcal{S}$.

The Monte Carlo importance sampling generates randomly a series of configurations $\mathcal{S}_1, \mathcal{S}_2, \mathcal{S}_3, ...$ that are distributed according to their weight $W(\mathcal{S}_i)$ which is called a Markov chain. The expectation value $\langle \mathcal{O} \rangle$ can then be calculated as the average over the values of the operator evaluated with those generated configurations

$$\langle \mathcal{O} \rangle = \lim_{N \to \infty} \frac{1}{N} \sum_{i=1}^{N} \mathcal{O}(\mathcal{S}_i). \tag{3.16}$$

To achieve that the configurations are distributed according to $W(\mathcal{S})$ two conditions need to be satisfied: ergodicity and detailed balance. Ergodicity requires that every configuration can be reached from every other configuration with a finite number of steps. Detailed balance means that the transition probabilities $p(\mathcal{S} \to \mathcal{S}')$ satisfy the following equation

$$W(\mathcal{S}) p(\mathcal{S} \to \mathcal{S}') = W(\mathcal{S}') p(\mathcal{S}' \to \mathcal{S}). \tag{3.17}$$

A new configuration $\mathcal{S}'$ is reached by proposing an update to the current configuration $\mathcal{S}$. This update is accepted or rejected with a certain probability. An acceptance probability that satisfies detailed balance is for example the heat bath probability

$$p(\mathcal{S} \to \mathcal{S}') = \frac{W(\mathcal{S}')}{W(\mathcal{S}) + W(\mathcal{S}') + const} \ . \tag{3.18}$$

3.3 Construction of the Loop Cluster Algorithm

The simplest algorithm for a Monte Carlo simulation is the Metropolis algorithm. However this algorithm can not be applied to simulate quantum spin systems since only one spin would be updated at once. For a quantum spin system this immediately results in a forbidden configuration and the proposed spin flips are always rejected. A solution would be that a whole plaquette is flipped at once but this would lead to very long autocorrelation times.

An algorithm that works very efficiently for quantum spin systems is the loop cluster algorithm. We have seen that the Hamiltonian acts locally on the level of the links. This means that detailed balance can be satisfied on the plaquettes. The idea of the loop cluster algorithm is to decorate the plaquettes with bond configurations. A bond is a straight line which connects two sites on a plaquette. If one flips two spins on a plaquette that are connected by a bond the spin configuration must remain valid. This means that only bonds that respect this condition can be chosen to decorate a plaquette. When all plaquettes are decorated with appropriate bonds one can build loops by starting at a random point in the lattice and following the bond lines. Since every site on the lattice is connected to two bonds this leads to a closed loop. The flip of

this loop automatically results in a valid configuration and updates the system in a nonlocal way. This leads to very short autocorrelation times. For every spin configuration on a plaquette there are different possibilities to set the bonds. The way these bonds are arranged on the plaquette is denoted as a breakup. It fixes the path that two potential incoming loops would have to take on the plaquette. For the different breakup possibilities have a look at figure 3.

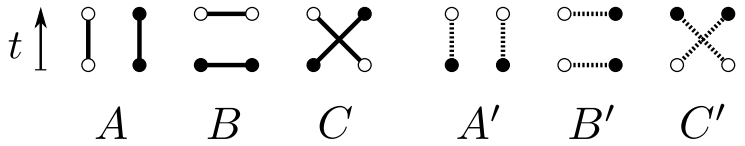

Figure 3: We use three different breakups the vertical, the horizontal and the diagonal breakup. The bonds connect either spins pointing in the same direction (A, B, C) or spins pointing in opposite directions (A', B', C').

One Monte Carlo update contains two steps. First we have to choose a breakup for all the active plaquettes. The probability to choose a breakup depends on the current spin configuration on the plaquette. The loops can now be built by following the bonds. The second step is to flip the loops. This means to invert the direction of each spin contained in the loop according to a probability. This probability depends usually on the Hamiltonian and the current spin configuration. In the models we consider the probability to flip a loop is always 1/2.

This procedure is describing a multi-cluster algorithm. There exists also a single-cluster variant of this algorithm which is described in section 3.7.

Here we want to give a more formal derivation of the loop algorithm. First we want to go from the spin model to a spin-bond model. The partition function is given as

$$Z = \sum_{\mathcal{S}} W(\mathcal{S}). \tag{3.19}$$

It only depends on the spin configuration $\mathcal{S}$. We introduce a new weight function $W(\mathcal{S}, b)$, that also depends on the bond configuration b. It has to satisfy

$$\sum_{b} W(\mathcal{S}, b) = W(\mathcal{S}), \qquad W(\mathcal{S}, b) \geq 0. \tag{3.20}$$

Because of the product structure of the weight $W(\mathcal{S}) = \prod_p W_p(S_p)$ we can go down to the plaquette level and perform the decomposition into different breakups separately on every plaquette. We then introduce the new weight $W_p(S_p, b_p)$ which is the weight of a plaquette with spins S_p and bonds b_p. It has to satisfy the same equation as $W(\mathcal{S}, b)$ does

$$\sum_{b_p} W_p(S_p, b_p) = W_p(S_p), \qquad W_p(S_p, b_p) \geq 0. \tag{3.21}$$

The weights $W_p(S_p)$ are already known from equation (3.12). To get the weights $W_p(S_p, b_p)$ we need to solve the system of equations given in the equation above. The breakup possibilities are denoted by A, B' and C. The A breakup connects two neighboring spins in the time direction. Both spins have to point in the same direction. The B' breakup connects two spins in a spacial direction. It is denoted with a prime since the connected spins have to point in opposite directions. The C breakup connects again two spins that point in the same direction but lie in the opposite corners of the plaquette. Consider Figure 3 for an example. Which breakup can be chosen on a plaquette p depends on the spin tupel $S_p = \{1^{\pm}, 2^{\pm}, 3^{\pm}\} = \{\begin{smallmatrix}\uparrow\uparrow\\\uparrow\uparrow\end{smallmatrix}, \begin{smallmatrix}\downarrow\downarrow\\\downarrow\downarrow\end{smallmatrix}, \begin{smallmatrix}\uparrow\downarrow\\\uparrow\downarrow\end{smallmatrix}, \begin{smallmatrix}\downarrow\uparrow\\\downarrow\uparrow\end{smallmatrix}, \begin{smallmatrix}\uparrow\downarrow\\\downarrow\uparrow\end{smallmatrix}, \begin{smallmatrix}\downarrow\uparrow\\\uparrow\downarrow\end{smallmatrix}\}$

$$\begin{aligned} W_p(1^{\pm}) &= e^{-\frac{a}{4}J'} &&= W(1^{\pm}, A) + W(1^{\pm}, C) &&= A + C, \\ W_p(2^{\pm}) &= e^{\frac{a}{4}J'} \cosh\left(\frac{a}{2}J\right) &&= W(2^{\pm}, A) + W(2^{\pm}, B') &&= A + B', \\ W_p(3^{\pm}) &= e^{\frac{a}{4}J'} \sinh\left(\frac{a}{2}|J|\right) &&= W(3^{\pm}, B') + W(3^{\pm}, C) &&= B' + C. \end{aligned} \tag{3.22}$$

This system of equations is under-determined, therefore we can impose that $W(S_{p_i}, X) = W(S_{p_j}, X)$, where p_i and p_j are plaquettes in the lattice and $X \in \{A, B', C\}$. Therefore we can write $W(S_p, X) = X$.

The weights for the specific models are calculated in section 3.6. The probability to choose a breakup b_p on a plaquette p with spins S_p is denoted as $p_{S,b}$ and given by

$$p_{S,b} = p(S_p \to (S_p, b_p)) = \frac{W_p(S_p, b_p)}{W_p(S_p)} \ . \tag{3.23}$$

Let us now summarize the steps for one update with the loop-cluster algorithm which are visualized in Figure 4.

- Choose a breakup on every active plaquette with the probability

$$p(S_p \to (S_p.b_p)) = \frac{W_p(S_p, b_p)}{W_p(S_p)}, \tag{3.24}$$

  and identify all the clusters.
- Flip all clusters separately with the probability 1/2.

3.4 Generalization of the Loop Cluster Algorithm for (2+1)-Dimensions

As already mentioned above this result can easily be generalized to higher dimensions. For a model in $(2+1)$-dimensions the Hamiltonian is split into four terms

$$\mathbb{H} = \mathbb{H}_1 + \mathbb{H}_2 + \mathbb{H}_3 + \mathbb{H}_4 \ , \tag{3.25}$$

which is showed in Figure 5. The four Hamiltonians act in a checkerboard pattern

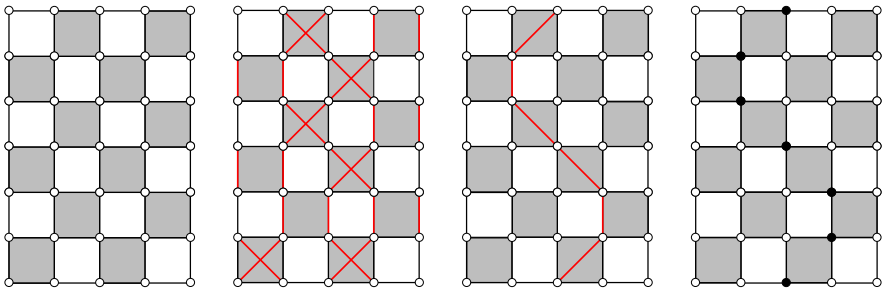

(a) (b) (c) (d)

Figure 4: Example for one update of the spin configuration with the loop-cluster algorithm for a 1-dimensional spin chain. White dots denote up spins and black dots down spins. Figure 4a a shows a spin configuration on a (1+1)-dimensional lattice where the Euclidean time is on the vertical axis and the spacial extent is on the horizontal axis. In Figure 4b we decorated the plaquettes with A and C breakups. Figure 4c shows one loop which is chosen randomly. By flipping the loop the new spin configuration, showed in Figure 4d, is generated.

$$\mathbb{H}_1 = \sum_{x\in(2m,n)} \mathbb{h}_{x,x+\hat{1}}, \qquad \mathbb{H}_2 = \sum_{x\in(m,2n)} \mathbb{h}_{x,x+\hat{2}}, \tag{3.26}$$

$$\mathbb{H}_3 = \sum_{x\in(2m+1,n)} \mathbb{h}_{x,x+\hat{1}}, \qquad \mathbb{H}_4 = \sum_{x\in(m,2n+1)} \mathbb{h}_{x,x+\hat{2}}. \tag{3.27}$$

Here, $\hat{i}$ for $i \in \{1,2\}$ denotes a unit vector in i direction. This leads to a different arrangement of the active plaquettes which is schematically shown in Figure 6. The rest of the algorithm stays the same. All the plaquette weights and flipping probabilities do not change.

3.5 Change of the Quantization Direction

With a unitary transformation we can change the quantization direction from the 3- to the 1-direction. This means that we have to change from a basis where σ_3 is diagonal to a basis where σ_1' is diagonal. The transformation matrix

$$u = \frac{1}{\sqrt{2}} \begin{pmatrix} 1 & 1 \\ i & -i \end{pmatrix}, \tag{3.28}$$

leads to a basis change such that

$$\sigma_1' = u\sigma_1 u^\dagger = \sigma_3, \qquad \sigma_2' = u\sigma_2 u^\dagger = \sigma_1, \qquad \sigma_3' = u\sigma_3 u^\dagger = \sigma_2, \tag{3.29}$$

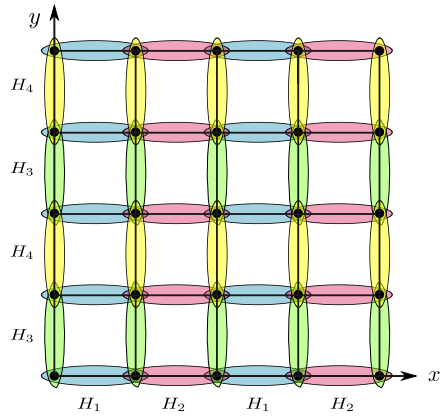

Figure 5: The Hamiltonian of the system is divided into four parts $\mathbb{H} = \mathbb{H}_1 + \mathbb{H}_2 + \mathbb{H}_3 + \mathbb{H}_4$. Each of the Hamiltonians acts on neighboring spin pairs.

where σ_1' is diagonal. To change the basis of a 2-spin state $|s_x s_y\rangle = |s_x\rangle \otimes |s_y\rangle$ we use the transformation matrix $U = u \otimes u$

$$U = \frac{1}{2}\begin{pmatrix} 1 & 1 & 1 & 1 \\ i & -i & i & -i \\ i & i & -i & -i \\ -1 & 1 & 1 & -1 \end{pmatrix}, \qquad U^\dagger = \frac{1}{2}\begin{pmatrix} 1 & -i & -i & -1 \\ 1 & i & -i & 1 \\ 1 & -i & i & 1 \\ 1 & i & i & -1 \end{pmatrix}. \tag{3.30}$$

The basis change from the 3- to the 1-basis leads to different allowed spin configurations on the plaquettes. Therefore also the plaquette weights $W(S_p)$ and the breakup possibilities change. This can be seen from the change of the transfer matrix

$$T^x = UT^zU^\dagger \tag{3.31}$$

$$= \begin{pmatrix} W(1^+) & 0 & 0 & W(4^-) \\ 0 & W(2^+) & W(3^-) & 0 \\ 0 & W(3^+) & W(2^-) & 0 \\ W(4^+) & 0 & 0 & W(1^-) \end{pmatrix} \tag{3.32}$$

$$= \begin{pmatrix} A+B+C & 0 & 0 & B \\ 0 & A & C & 0 \\ 0 & C & A & 0 \\ B & 0 & 0 & A+B+C \end{pmatrix}, \tag{3.33}$$

where $W(4^\pm) = \langle\uparrow\uparrow| e^{-a\mathbb{h}_{x,x+\hat{1}}} |\downarrow\downarrow\rangle = \langle\downarrow\downarrow| e^{-a\mathbb{h}_{x,x+\hat{1}}} |\uparrow\uparrow\rangle$ is a spin configuration that was forbidden when we used the 3-direction as the quantization axis. The B'-breakup has changed into a B-breakup which connects parallel spins . So all the spins in a cluster point in the same direction.

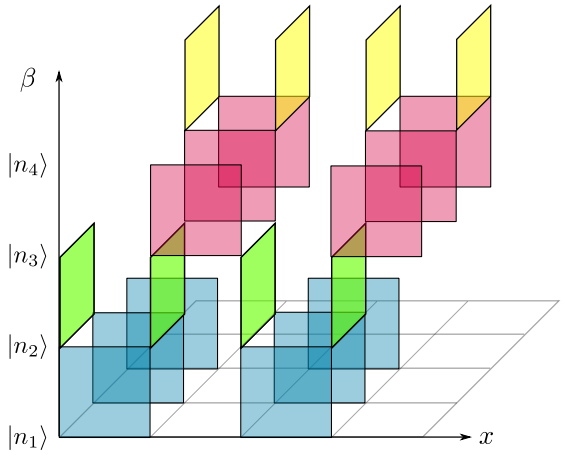

Figure 6: The Hamiltonians acts in a 3-dimensional checkerboard pattern. One lattice spacing contains four time-steps $a = 4\Delta\tau$.

3.6 Breakup Probabilities for the Different Models

3.6.1 Heisenberg Anti-Ferromagnet

Let us consider the Heisenberg anti-ferromagnet in the 3-basis. In this model the parameter is $J = J' > 0$. The allowed spin configurations on a plaquette, their weights and the possible breakups are

$$\begin{array}{lll} \begin{smallmatrix}\uparrow & \uparrow\\ \uparrow & \uparrow\end{smallmatrix} = e^{-\frac{a}{4}J} & = A + C, \\ \begin{smallmatrix}\uparrow & \downarrow\\ \uparrow & \downarrow\end{smallmatrix} = \frac{1}{2}e^{-\frac{a}{4}J}(1+e^{aJ}) & = A + B', \\ \begin{smallmatrix}\uparrow & \downarrow\\ \downarrow & \uparrow\end{smallmatrix} = \frac{1}{2}e^{-\frac{a}{4}J}(1-e^{aJ}) & = B' + C, \end{array} \tag{3.34}$$

where $\begin{smallmatrix}\uparrow & \uparrow\\ \uparrow & \uparrow\end{smallmatrix}$ denotes the weight $W_p(1^{\pm})$ of a plaquette with this spin configuration or with the flipped configuration $\begin{smallmatrix}\downarrow & \downarrow\\ \downarrow & \downarrow\end{smallmatrix}$. For the other configuration the meaning is defined analogously. This leads to the following weights for the breakups

$$A = e^{-\frac{a}{4}J}, \qquad B' = \frac{1}{2}e^{-\frac{a}{4}J}(-1+e^{-aJ}), \qquad C = 0. \tag{3.35}$$

With these weights we calculate the probabilities with which a specific breakup is chosen for a spin configuration S_p on a plaquette. The C-breakup does not occur for this model

$$\begin{aligned} p_{1,A} &= 1, & p_{2,A} &= \frac{2}{1+e^{aJ}}, \\ p_{3,B'} &= 1, & p_{2,B'} &= \tanh(\frac{aJ}{2}). \end{aligned} \tag{3.36}$$

3.6.2 Heisenberg Ferromagnet

The Heisenberg ferromagnet is also considered in the 3-basis. Here we have $J = J' < 0$. The allowed spin configurations on a plaquette, their weights and the possible breakups are

$$\begin{array}{ll} \uparrow\uparrow \\ \uparrow\uparrow \end{array} = e^{-\frac{a}{4}J} = A + C, \qquad \begin{array}{ll} \uparrow\downarrow \\ \uparrow\downarrow \end{array} = \frac{1}{2}e^{\frac{3a}{4}J}(1 + e^{-aJ}) = A + B', \qquad \begin{array}{ll} \uparrow\downarrow \\ \downarrow\uparrow \end{array} = \frac{1}{2}e^{\frac{3a}{4}J}(-1 + e^{-aJ}) = B' + C, \tag{3.37}$$

which leads to the following breakup weights

$$A = \frac{1}{2}e^{\frac{3a}{4}J}, \qquad B' = 0, \qquad C = \frac{1}{2}e^{\frac{3a}{4}J}(-1 + e^{-aJ}). \tag{3.38}$$

In this model the B-breakup vanishes. The probabilities for the breakups are

$$p_{1,A} = \frac{1}{2}(1 + e^{aJ}), \qquad p_{2,A} = 1$$
$$p_{1,C} = \frac{1}{2}(1 - e^{aJ}), \qquad p_{3,C} = 1. \tag{3.39}$$

3.6.3 XY-Model

For the XY-model we have that $J' = 0$. We consider the XY-model in the 1-basis since the order parameter of the system lies in the $(1, 2)$-plane. The allowed spin configurations on a plaquette, their weights and breakup possibilities are

$$\begin{array}{ll} \uparrow\uparrow \\ \uparrow\uparrow \end{array} = \frac{1}{2}(1 + e^{\frac{a}{2}|J|}) = A + B + C, \qquad \begin{array}{ll} \uparrow\downarrow \\ \uparrow\downarrow \end{array} = \frac{1}{2}(1 + e^{-\frac{a}{2}|J|}) = A, \qquad \begin{array}{ll} \uparrow\downarrow \\ \downarrow\uparrow \end{array} = \frac{1}{2}(1 - e^{-\frac{a}{2}|J|}) = C, \qquad \begin{array}{ll} \uparrow\uparrow \\ \downarrow\downarrow \end{array} = \frac{1}{2}(-1 + e^{\frac{a}{2}|J|}) = B'. \tag{3.40}$$

The weights for the breakups are

$$A = \frac{1}{2}(1 + e^{-\frac{a}{2}|J|}), \qquad B = \frac{1}{2}(-1 + e^{\frac{a}{2}|J|}), \qquad C = \frac{1}{2}(1 - e^{-\frac{a}{2}|J|}), \tag{3.41}$$

which leads to the probabilities

$$p_{1,A} = e^{-\frac{a}{2}|J|}, \qquad p_{2,A} = 1,$$
$$p_{1,B} = \tanh(\frac{a}{4}|J|), \qquad p_{3,C} = 1,$$
$$p_{1,C} = e^{-\frac{a}{2}|J|}\tanh(\frac{a}{4}|J|), \qquad p_{4,B} = 1\ . \tag{3.42}$$

3.7 Single-Cluster Variant

In the previous sections we described the loop cluster algorithm in a multi-cluster variant. The multi-cluster algorithm chooses first a breakup for every plaquette and then builds the clusters according to this choice. The computation time is therefore proportional to the volume of the lattice. The idea of the single cluster algorithm is to construct only one loop. For the construction of this loop we start on a random site $s = (x_0, t_0)$ at plaquette p_0 and we choose the breakup only for the current plaquette. Then by following the bond we reach the next plaquette and choose the breakup for this plaquette. This step is repeated until the loop is closed. The computational effort is therefore proportional to the length of the loop. The probability to flip this cluster is 1 instead of 1/2. For the single cluster algorithm it is more likely to pick an initial site out of a large cluster than to pick one out of a small cluster. This leads to big changes in the phase space during one update which can reduce critical slowing down further. Whether the multi-cluster algorithm or the single-cluster algorithm is more efficient depends on the measured observable.

3.8 Detailed Balance and Ergodicity

The cluster algorithm needs to satisfy detailed balance and ergodicity to work properly.

Detailed Balance

For detailed balance we need to satisfy equation (3.17). We show this equality in two steps. First we show that the update of the spins satisfies detailed balance and then we show that the update of the bond also satisfies the equation.

The probability to flip a cluster $\mathscr{C}$ is given by the heat bath probability

$$p_{flip} = \frac{W(\mathscr{C}')}{W(\mathscr{C}) + W(\mathscr{C}')}, \tag{3.43}$$

where $W(\mathscr{C}) = \prod_{p\in\mathscr{C}} W(S_p, b_p)$ and $W(\mathscr{C}') = \prod_{p\in\mathscr{C}} W(S'_p, b_p)$. Since we enforce that the weight of a cluster remains the same when we flip the spins

$$\prod_{p\in\mathscr{C}} W_p(S_p, b) = \prod_{p\in\mathscr{C}} W_p(S'_p, b) \tag{3.44}$$

the probability p_{flip} is always 1/2 and therefore the update of the spin configuration from $\mathcal{S} \to \mathcal{S}'$ satisfies detailed balance

$$W(\mathcal{S}, b)p_{flip} = W(\mathcal{S}', b)p_{flip}. \tag{3.45}$$

The probability to update the bonds b_p on a plaquette p with spins S_p is given by

$$p((S_p, b_p) \to (S_p.b'_p)) = \frac{W_p(S_p, b'_p)}{W_p(S_p)}\ . \tag{3.46}$$

This is also a heat bath probability and satisfies detailed balance by construction

$$W(\mathcal{S}, b)p((S, b) \to (S, b')) = W(\mathcal{S}, b')p((S, b') \to (S.b)). \tag{3.47}$$

Ergodicity

Ergodicity has to be shown for every model separately. For the XY-model in the 1-basis ergodicity is obvious since all breakup possibilities A, B and C have non vanishing weights.

For the Heisenberg Ferro- and Antiferromagnet in the 3-basis the easiest way to see ergodicity is by introducing the worldline picture. A worldline is a possibility to describe a spin configuration on the checkerboard lattice. It is like a loop which is only built by A and C breakups. At every site touched by the loop sits an up spin and at all the empty sites sit down spins.

For the Heisenberg ferromagnet we only have A and C breakups. Any worldline configuration can be covered with those A and C breakups. Flipping all the loops, that lie on the worldline, results in an empty worldline configuration. Reversely any configuration can be created out of the empty worldline configuration. This means that every configuration can be transformed to any other configuration within two Monte Carlo steps.

For the Heisenberg antiferromagnet only the A and the B breakup have a non-vanishing weight. The reference configuration for this model is not the empty one but the staggered configuration. To reach a staggered configuration we need to be on a bipartite lattice. The configuration is then built by putting vertical worldlines on one of the two sub-lattices.

For any worldline configuration there exists a unique bond configuration to reach the staggered worldline configuration. To reach this unique bond configuration we covered vertical worldlines with an A breakup and diagonal worldlines with a B breakup. By flipping the right loops the staggered configuration is reached. For the Heisenberg antiferromagnet any configuration can be reached by any other if we are on a bipartite lattice. The algorithm is ergodic for all models that we consider.

3.9 Observables in Euclidean-Time

To calculate the expectation value of an operator $\langle \mathcal{O} \rangle$ one takes the average over the values of the operator evaluated for every possible spin configuration $\mathcal{S}_n$ of the system

$$\langle \mathcal{O} \rangle = \lim_{N \to \infty} \frac{1}{N} \sum_{i=1}^{N} \mathcal{O}(\mathcal{S}_i). \tag{3.48}$$

There are different observables we can calculate in a quantum spin system. Let us assume we quantized the system in the 1-direction. This means that we are in a basis where the spin operator S_x^1 is diagonal. The uniform magnetization is then given as

$$\mathcal{M} = \sum_{x \in \Lambda} S_x^1, \tag{3.49}$$

where x is a coordinate of the $(d+1)$-dimensional lattice Λ. S^1_x denotes the first component of the spin at site x. The susceptibility is given as

$$\begin{aligned}\chi &= \frac{1}{V}\left\langle S^1_{\vec{x}}(t) S^1_{\vec{y}}(t')\right\rangle \\ &= \frac{1}{V}\Big\langle \sum_{t,t'}\sum_{\vec{x},\vec{y}} S^1_{\vec{x}}(t) S^1_{\vec{y}}(t')\Big\rangle \\ &= \frac{1}{V}\Big\langle \Big(\sum_{t}\sum_{\vec{x}} S^1_{\vec{x}}(t)\Big)^2\Big\rangle \\ &= \frac{1}{V}\left\langle \mathcal{M}^2\right\rangle, \end{aligned} \tag{3.50}$$

where $\vec{x}$ denotes the spacial coordinate in d dimensions. If we are in a phase with $T < T_C$, where T_C is the critical temperature, then χ is of the order of V. In the multi-cluster algorithm we can derive an improved estimator for the susceptibility

$$\begin{aligned}\chi &= \frac{1}{V}\Big\langle \Big(\sum_{\vec{x}} S^1_x\Big)^2\Big\rangle \\ &= \frac{1}{V}\Big\langle \Big(\sum_{\mathscr{C}}\sum_{x\in\mathscr{C}} S^1_x\Big)^2\Big\rangle . \end{aligned} \tag{3.51}$$

We define $\mathcal{M}^1_{\mathscr{C}} = \sum_{x\in\mathscr{C}} S^1_x$ and write out the square term. This leads to

$$\begin{aligned}\chi &= \frac{1}{V}\Big\langle \sum_{\mathscr{C}_1}\mathcal{M}^1_{\mathscr{C}_1}\sum_{\mathscr{C}_2}\mathcal{M}^1_{\mathscr{C}_2}\Big\rangle \\ &= \frac{1}{V}\Big\langle \sum_{\mathscr{C}}\left(\mathcal{M}^1_{\mathscr{C}}\right)^2\Big\rangle . \end{aligned} \tag{3.52}$$

In the second step we used that the clusters are uncorrelated. The only term that is not canceled in the sum over all clusters and all configurations is the term where $\mathscr{C}_1 = \mathscr{C}_2$. Since we quantized the system in the 1-direction all spins in a cluster point in the same direction. Therefore $\left(\mathcal{M}^1_{\mathscr{C}_1}\right)^2 = \left(\sum_x |S^1_x|\right)^2 = |\mathscr{C}|^2$, where $|\mathscr{C}|$ denotes the length of the cluster, and we can write

$$\chi = \frac{1}{V}\Big\langle \sum_{\mathscr{C}} |\mathscr{C}|^2\Big\rangle_{MC} . \tag{3.53}$$

We can also adapt this improved estimator for the single-cluster algorithm. In the single-cluster algorithm large clusters are preferred. The probability for a single cluster to be built is proportional to its size

$$p_{\mathscr{C}} = \frac{|\mathscr{C}|}{V}. \tag{3.54}$$

The susceptibility for the single cluster is therefore

$$\begin{aligned} \chi &= \frac{1}{V}\Big\langle \frac{|\mathscr{C}|^2}{p_{\mathscr{C}}} \Big\rangle \\ &= \langle\, |\mathscr{C}|\, \rangle_{SC} \ . \end{aligned} \tag{3.55}$$

In the single cluster algorithm the susceptibility is proportional to the cluster size. This improved estimator is also valid if the system is quantized in the 3-direction.

4 Real-Time Evolution of a Quantum Spin System

The reason why we want to simulate the evolution of a quantum spin system in real time with a Monte Carlo procedure is because for large systems it is not possible to calculate the evolution analytically. The time evolution of a quantum state is generally given by

$$|\Psi(t)\rangle = U(t,t_0)\,|\Psi(t_0)\rangle\,, \qquad U(t,t_0) = \mathrm{T}e^{-i\int_{t_0}^{t}\mathbb{H}(t')dt'}, \tag{4.1}$$

where $U(t_0,t)$ is a unitary time evolution operator and T is the time ordering operator. For the case where the Hamiltonian is time-independent $\mathbb{H}(t) = \mathbb{H}$ the time evolution operator is

$$U(t_0,t) = e^{-i\mathbb{H}(t-t_0)}, \tag{4.2}$$

where $U(t_f,t_0)$ has the property

$$U(t_f,t_0) = U(t_f,t)U(t,t_0). \tag{4.3}$$

To calculate the exponential of the Hamiltonian one has to diagonalize it. The problem is that the dimension of the Hilbert space grows exponentially with the volume of the system and therefore the Hamiltonian cannot be diagonalized for large systems.

However, the standard Monte Carlo procedure does not work for this unitary time evolution since we have complex weights in the path integral. Therefore we decided to investigate another more manageable problem. For this simulation the evolution is entirely driven by measurements, either by sporadic measurements or by continuous monitoring by a Lindblad process. We found three different measurement processes that don't suffer from a sign problem if we sum over the intermediate measurement results. The Hamiltonian is set to zero for the whole real time evolution such that $U(t_f,t_i) = \mathbb{1}$.

In this section we derive the path integral formalism for the real time evolution of the density matrix ρ. Together with the preparation of this initial density matrix we obtain a path integral along a Keldysh contour. We will then derive cluster rules to simulate the system in real time with a loop-cluster algorithm. This extends the loop-cluster algorithm from the euclidean part with the real-time part. This section is mainly based on [12, 13].

4.1 The Density operator

This subsection is based on [14, 15]. The density operator of a quantum system which is described by an ensemble of states $\{|\psi_i\rangle\}$ with probabilities p_i is given as

$$\rho = \sum_i p_i\,|\psi_i\rangle\,\langle\psi_i|\,, \tag{4.4}$$

where $\sum_i p_i = 1$. In any complete set of orthonormal basis states it can be represented as a matrix, the density matrix, whose elements are

$$\rho_{ij} = \langle i| \rho |j\rangle . \tag{4.5}$$

The density matrix is Hermitean $\rho = \rho^\dagger$ which implies that its eigenvalues are real. If the states $|\psi_i\rangle$ are orthonormal the eigenvalues are just the probabilities p_i and the density matrix is normalized to

$$\mathrm{Tr}[\rho] = \sum_j \langle j|\rho|j\rangle = \sum_i p_i \sum_j \langle j|\psi_i\rangle \langle\psi_i|j\rangle = \sum_i p_i = 1. \tag{4.6}$$

For a canonical ensemble described by the Hamiltonian $\mathbb{H}$ the density matrix is given by

$$\rho = \frac{1}{Z} e^{-\beta \mathbb{H}} = \frac{1}{Z} \sum_n e^{-\beta E_n} |n\rangle \langle n| , \tag{4.7}$$

where $\mathbb{H}|n\rangle = E_n |n\rangle$. With the density matrix we can easily calculate the expectation value of an observable which is represented by the operator $\mathcal{O}$.

$$\begin{aligned} \langle \mathcal{O} \rangle &= \sum_i p_i \langle \psi_i| \mathcal{O} |\psi_i\rangle = \sum_{j,k} \sum_i p_i \langle \psi_i|k\rangle \langle k| \mathcal{O} |j\rangle \langle j|\psi_i\rangle = \sum_{j,k} \rho_{jk} \mathcal{O}_{jk} \\ &= \mathrm{Tr}[\mathcal{O}\rho]. \end{aligned} \tag{4.8}$$

4.1.1 The Real-Time Dynamics of the Density Operator

The real time dynamics of a density operator is described by the von Neumann equation

$$i \frac{\partial \rho}{\partial t} = [\mathbb{H}, \rho] . \tag{4.9}$$

This differential equation is solved by

$$\rho(t) = U(t, t_0) \rho(t_0) U(t_0, t), \tag{4.10}$$

where $U(t, t_0) = U(t_0, t)^\dagger$ is the unitary time-evolution operator described in equation (4.2). The density matrix can also be evolved in time by measurements. If we perform a measurement of an observable $\mathcal{O}$ on a quantum system the probability to obtain a measurement result o_k is

$$p_{o_k} = \sum_{i_{o_k}} \langle i_{o_k}| \rho |i_{o_k}\rangle = \mathrm{Tr}[P_{o_k} \rho], \tag{4.11}$$

where $|i_{o_k}\rangle$ are all the eigenvectors of the operator $\mathcal{O}$ with eigenvalue o_k. P_{o_k} denotes the projection operator that projects on the subspace of the Hilbert space spanned by the eigenvectors of $\mathcal{O}$ with eigenvalue o_k

$$P_{o_k} = \sum_{i_{o_k}} |i_{o_k}\rangle \langle i_{o_k}| . \tag{4.12}$$

The density matrix after a measurement described by the projection operator P_{o_k} is

$$\rho' = P_{o_k} \rho P_{o_k}. \tag{4.13}$$

4.2 The Real-Time Path Integral

We are now interested in the probability to reach a final state $|f\rangle$ at time t_f, after a sequence of N sporadic measurements with results o_k, when starting with an initial density matrix $\rho_0 = \sum_i p_i |i\rangle \langle i| = \frac{1}{Z} e^{-\beta \mathbb{H}_0}$ at time t_0. This density matrix describes a system in thermal equilibrium with an inverse temperature $\beta = \frac{1}{T}$

$$\begin{aligned} p_{\rho_0, f}(o_1, o_2, ..., o_N) \; = \; & \langle f | \, U(t_f, t_N) P_{o_N} ... P_{o_2} U(t_2, t_1) P_{o_1} U(t_1, t_i) \rho_0 \\ & \cdot U(t_0, t_1) P'_{o_1} U(t_1, t_2) P'_{o_2} ... P'_{o_N} U(t_N, t_f) \, |f\rangle \, . \end{aligned} \tag{4.14}$$

The prime in P'_{o_k} indicates that the projection operator acts on the forward branch. The expression above is defined along a closed contour in the complex time plane. If we look at this expression we can identity a backward branch on the real-time axis from state $|f\rangle$ at time t_f to the time t_i, a branch in the Euclidean time direction from time t_i to the euclidean time $i\beta$ that results from the density matrix $\rho_0 = \frac{1}{Z} e^{-\beta \mathbb{H}_0} = U(0, i\beta)$ and a forward branch from t_i back to time t_f. This closed contour is called a Keldysh contour [16] and is shown in Figure 7.

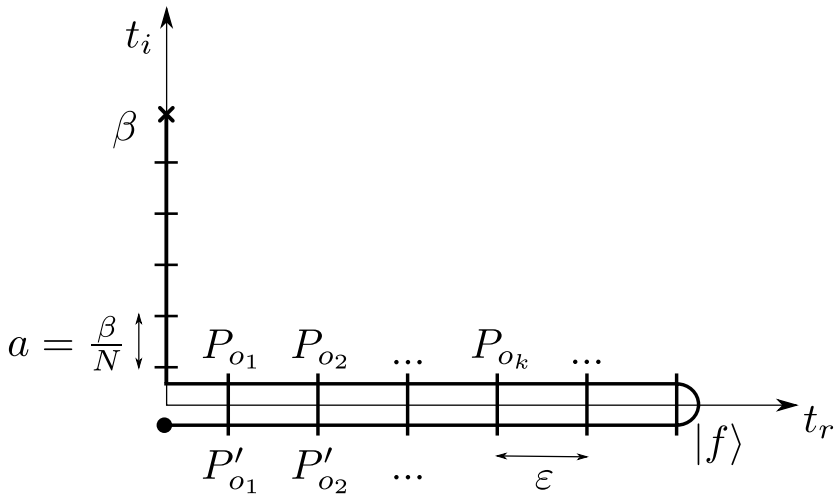

Figure 7: The Keldysh Contour in the complex time-plane.

We set the Hamiltonian to zero, which means that the time-evolution operator $U(t, t') = \mathbb{1}$. To obtain a path integral formulation we insert complete sets of states $\mathbb{1} = \sum_{n_i} |n_i\rangle \langle n_i|$ in the forward branch and $\mathbb{1} = \sum_{n'_i} |n'_i\rangle \langle n'_i|$ in the

backward branch

$$p_{\rho_0,f}(o_1,o_2,...,o_N) = \sum_i p_i \sum_{\substack{n_1,..,n_{N-1}\\ n'_1,..,n'_{N-1}}} \langle i|P_{o_1}\,|n_1\rangle\,\langle n_1|\,P_{o_2}\,|n_2\rangle\,...\,\langle n_{N-1}|\,P_{o_N}\,|f\rangle \cdot \langle f|P'_{o_N}\,|n'_{N-1}\rangle\,...\,\langle n'_2|\,P'_{o_2}\,|n'_1\rangle\,\langle n'_1|\,P'_{o_1}|i\rangle\,. \tag{4.15}$$

We can write this expression in a doubled Hilbert space of states. This means that we combine the state $|n_k\rangle$ at time t_k from the forward branch with the state $|n'_k\rangle$ at time t_k from the backward branch such that

$$\langle n_{k-1}|\,P_{o_k}\,|n_k\rangle\,\langle n'_k|\,P'_{o_k}\,|n_{k-1'}\rangle = \langle n_{k-1}n'_{k-1}|\,P_{o_k}\otimes P^*_{o_k}\,|n_k n'_k\rangle\,. \tag{4.16}$$

Since we are interested in the probability of reaching a final state $|f\rangle$ irrespective of all the intermediate measurement results we perform a sum over all the possible measurement results o_k of the operator P_{o_k}. This leads to the following expression for the path integral

$$\begin{aligned} &p_{\rho_0,f}\\ &= \sum_{o_1,..o_N}\sum_i p_i \sum_{\substack{n_1,..,n_{N-1}\\ n'_1,..,n'_{N-1}}} \langle ii|\,P_{o_1}\otimes P^*_{o_1}\,|n_1n'_1\rangle\,...\,\langle n_{N-1}n'_{N-1}|\,P_{o_N}\otimes P^*_{o_N}\,|ff\rangle\\ &= \sum_i p_i \sum_{\substack{n_1,..,n_{N-1}\\ n'_1,..,n'_{N-1}}} \prod_{k=1}^{N} \langle n_{k-1}n'_{k-1}|\,\tilde{\mathbb{P}}_k\,|n_k n'_k\rangle\,. \end{aligned} \tag{4.17}$$

We use that $\langle ii| = \langle n_0 n'_0|$ and $|ff\rangle = |n_N n'_N\rangle$. The operator $\tilde{\mathbb{P}}_k$ is defined as

$$\tilde{\mathbb{P}}_k = \sum_{o_k} P_{o_k}\otimes P^*_{o_k}. \tag{4.18}$$

If it is positive definite all the weights used for Monte Carlo importance sampling are positive and it is therefore possible to simulate the real-time evolution of the system driven by the measurements P_{o_k}.

In one time step we will always perform a sequence of measurements on pairs of neighboring spins. The measurement process consists of sequences of four steps. In a first step the spins at site $\vec{x} = (x_1, x_2)$ with even x_1 and their nearest neighbors in the $\hat{1}$-direction are measured. In a second step we measure spins at sites with even x_2 and their nearest neighbors in the $\hat{2}$-direction. The next two steps are again the same but with odd x_1 for the third step and odd x_2 for the fourth step. This measurement sequence is repeated an arbitrary number of times. This gives us the same checker board pattern as for the loop-cluster algorithm showed in Figure 6. The transfer matrix element can then be written as a product over all nearest neighbor spin pairs. In the doubled Hilbert space

this is

$$\langle n_{k-1} n'_{k-1}| \, \tilde{\mathbb{P}}_k \, |n_k n'_k\rangle = \prod_{\langle xy\rangle} \langle s_{x,k-1} s_{y,k-1} s'_{x,k-1} s'_{y,k-1}| \, \tilde{\mathbb{P}} \, |s_{x,k} s_{y,k} s'_{x,k} s'_{y,k}\rangle \, . \tag{4.19}$$

The products over k and $\langle xy\rangle$ can be combined to a product over all active plaquettes p. The path integral is then given by

$$p_{\rho_0,f} = \sum_i p_i \sum_{\substack{n_1,..,n_{N-1} \\ n'_1,..,n'_{N-1}}} \prod_p \langle s_{x,k-1} s_{y,k-1} s'_{x,k-1} s'_{y,k-1}| \, \tilde{\mathbb{P}} \, |s_{x,k} s_{y,k} s'_{x,k} s'_{y,k}\rangle \, . \tag{4.20}$$

As in the Euclidean path integral the transfer matrix defines the weights of the spin configurations on a plaquette and therefore also determines the cluster rules for the loop-cluster algorithm.

4.3 The Loop-Cluster Algorithm in Real Time

We derived a path integral expression for the probability to reach a final state $|f\rangle$ when starting from an initial density matrix ρ_0. We want to calculate this probability with a loop-cluster algorithm. The initial density matrix is defined according to the anti-ferromagnetic Heisenberg model, the ferromagnetic Heisenberg model or the XY-model. It is calculated with a simulation in Euclidean time that we have seen before. The real-time evolution then starts from one time slice in the lattice of the simulation of ρ_0. This means that we attach the two real-time lattices to one time slice of the Euclidean lattice, one for the forward branch and one for the backward branch. They are closed through periodic boundary conditions. To construct a cluster we first start drawing a loop in the Euclidean part of the lattice according to the cluster rules of the model we have chosen. When we reach a site that lies in the starting time slice of the real-time lattice we go on building the loop according to the cluster rules of the measurement process. The loop continues growing in the lattices for the forward and backward branch and returns to the Euclidean lattice to continue the Euclidean loop. In Figure 8 this is shown graphically for a 1-d spin chain. This procedure also samples over all the final states $|f\rangle$. One can implement the loop-cluster algorithm in a single- or in a multi-cluster variant. For the single-cluster algorithm only one cluster is built at the same time but it is flipped with probability 1. For the multi-cluster variant one has to build all the loops which are then flipped independently with probability 1/2.

4.4 Measurement Processes

We found three different measurement processes to evolve a quantum spin system in real time that do not cause a sign problem.

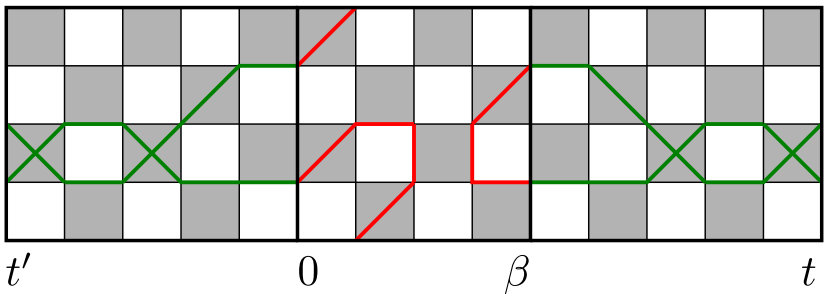

Figure 8: The red line builds a cluster in the Euclidean time. The green line shows the continuation of the Euclidean cluster in real time. The real-time cluster is symmetric on the forward and on the backward branch.

4.4.1 Measurement Process: $\mathcal{O}_1 = (\vec{S}_x + \vec{S}_y)^2$

This process measures the total spin $S = (\vec{S}_x + \vec{S}_y)^2$ of two neighboring spins at the sites x and y. This measurement conserves the magnetization $\mathcal{M} = \sum_{z\in\Lambda} S_z^3$ of the system

$$\left[\vec{S}^2, \mathcal{M}\right] = 0. \tag{4.21}$$

The total spin operator S has four eigenstates denoted by $|SS^3\rangle$ where S^3 is the 3-component of the spin.

$$\begin{aligned} |11\rangle &= \uparrow\uparrow, \\ |10\rangle &= \frac{1}{\sqrt{2}}(\uparrow\downarrow + \downarrow\uparrow), \\ |1-1\rangle &= \downarrow\downarrow, \\ |00\rangle &= \frac{1}{\sqrt{2}}(\uparrow\downarrow - \downarrow\uparrow). \end{aligned} \tag{4.22}$$

We can distinguish two projection operators since the total spin has two eigenvalues $S = 1$ and $S = 0$. The projection operator for the measurement result 0 is $P_0 = |00\rangle\langle 00|$ and the projection operator for the measurement result 1 is $P_1 = |11\rangle\langle 11| + |10\rangle\langle 10| + |1-1\rangle\langle 1-1|$. In a matrix representation according to equation (2.8) the projection operators are written as

$$P_0 = \begin{pmatrix} 0 & 0 & 0 & 0 \\ 0 & \frac{1}{2} & -\frac{1}{2} & 0 \\ 0 & -\frac{1}{2} & \frac{1}{2} & 0 \\ 0 & 0 & 0 & 0 \end{pmatrix}, \qquad P_1 = \begin{pmatrix} 1 & 0 & 0 & 0 \\ 0 & \frac{1}{2} & \frac{1}{2} & 0 \\ 0 & \frac{1}{2} & \frac{1}{2} & 0 \\ 0 & 0 & 0 & 1 \end{pmatrix}. \tag{4.23}$$

The projection operator P_0 would cause a sign problem but we will see that the transfer matrix $\tilde{\mathbb{P}} = P_0 \otimes P_0^* + P_1 \otimes P_1^*$ is positive definite. It is given by a

16×16-matrix whose elements can be written as a product of Kronecker deltas

$$\begin{aligned}
&\langle s_{x,k-1} s_{y,k-1} s'_{x,k-1} s'_{y,k-1}| \, \tilde{\mathbb{P}} \, |s_{x,k} s_{y,k} s'_{x,k} s'_{y,k}\rangle \\
&= \frac{1}{2}(\delta_{s_{x,k-1},s_{x,k}} \delta_{s_{y,k-1},s_{y,k}} \delta_{s'_{x,k-1},s'_{x,k}} \delta_{s'_{y,k-1},s'_{y,k}} \\
&\quad + \delta_{s_{x,k-1},s_{y,k}} \delta_{s_{y,k-1},s_{x,k}} \delta_{s'_{x,k-1},s'_{y,k}} \delta_{s'_{y,k-1},s'_{x,k}}).
\end{aligned} \tag{4.24}$$

From these matrix elements one obtains the allowed spin configurations on a plaquette and their weights. In the expression above we see that the clusters and therefore also the spins are identical on the forward and on the backward branch of the Keldysh contour. We can therefore neglect one branch for the simulation and the above expression simplifies to

$$\langle s_{x,k-1} s_{y,k-1}| \, \tilde{P} \, |s_{x,k} s_{y,k}\rangle = \frac{1}{2}(\delta_{s_{x,k-1},sx,k} \delta_{s_{y,k-1},s_{y,k}} + \delta_{s_{x,k-1},sy,k} \delta_{s_{y,k-1},s_{x,k}}).$$

It turns out that the matrix $\tilde{P}$ is equal to the projection operator P_1.

4.4.2 Measurement Process: $\mathcal{O}_2 = S^1_x S^1_y$

$S^1_x S^1_y$ measures the product of the two first components of the spins at the sites x and y. If the two spins are parallel the measurement result is +1 and if they are anti-parallel the measurement result is -1. This measurement process does neither conserve the uniform magnetization nor the staggered magnetization. The matrix representation of the measurement process is

$$S^1_x S^1_y = \begin{pmatrix} 0 & 0 & 0 & 1 \\ 0 & 0 & 1 & 0 \\ 0 & 1 & 0 & 0 \\ 1 & 0 & 0 & 0 \end{pmatrix}. \tag{4.25}$$

We obtain two projection operators since the measurement has two possible results. The eigenstates corresponding to the measurement result +1 are

$$EV_1 = \frac{1}{\sqrt{2}}(|\uparrow\uparrow\rangle + |\downarrow\downarrow\rangle), \qquad EV_2 = \frac{1}{\sqrt{2}}(|\uparrow\downarrow\rangle + |\downarrow\uparrow\rangle), \tag{4.26}$$

and for the measurement result -1 they are

$$EV_3 = \frac{1}{\sqrt{2}}(|\uparrow\uparrow\rangle - |\downarrow\downarrow\rangle), \qquad EV_4 = \frac{1}{\sqrt{2}}(|\uparrow\downarrow\rangle - |\downarrow\uparrow\rangle). \tag{4.27}$$

In a matrix representation the projection operators are

$$P_1 = \frac{1}{2}\begin{pmatrix} 1 & 0 & 0 & 1 \\ 0 & 1 & 1 & 0 \\ 0 & 1 & 1 & 0 \\ 1 & 0 & 0 & 1 \end{pmatrix}, \qquad P_{-1} = \frac{1}{2}\begin{pmatrix} 1 & 0 & 0 & -1 \\ 0 & 1 & -1 & 0 \\ 0 & -1 & 1 & 0 \\ -1 & 0 & 0 & 1 \end{pmatrix}. \tag{4.28}$$

The operator $P_{-1} \otimes P_{-1}^*$ would again give rise to a sign problem. However, since we sum over all measurement results the elements of the transfer matrix $\tilde{\mathbb{P}} = P_1 \otimes P_1^* + P_{-1} \otimes P_{-1}^*$ are positive. They can again be written as a product of Kronecker deltas

$$\begin{aligned}
&\langle s_{x,k-1} s_{y,k-1} s'_{x,k-1} s'_{y,k-1} |\, \tilde{\mathbb{P}} \,| s_{x,k} s_{y,k} s'_{x,k} s'_{y,k} \rangle \\
&= \frac{1}{2} (\delta_{s_{x,k-1}, s_{x,k}} \delta_{s_{y,k-1}, s_{y,k}} \delta_{s'_{x,k-1}, s'_{x,k}} \delta_{s'_{y,k-1}, s'_{y,k}} \\
&\quad + \delta_{s_{x,k-1}, -s_{x,k}} \delta_{s_{y,k-1}, -s_{y,k}} \delta_{s'_{x,k-1}, -s'_{x,k}} \delta_{s'_{y,k-1}, -s'_{y,k}}).
\end{aligned} \tag{4.29}$$

As before we can neglect one branch of the Keldysh contour since the clusters on the forward and on the backward branch are identical. The transfer matrix simplifies to

$$\tilde{\mathrm{P}} = \begin{pmatrix} \frac{1}{2} & 0 & 0 & \frac{1}{2} \\ 0 & \frac{1}{2} & \frac{1}{2} & 0 \\ 0 & \frac{1}{2} & \frac{1}{2} & 0 \\ \frac{1}{2} & 0 & 0 & \frac{1}{2} \end{pmatrix}. \tag{4.30}$$

4.4.3 Measurement Process: $\mathcal{O}_3 = S_x^+ S_y^+ + S_x^- S_y^-$

For this measurement process we introduce the raising and lowering operators $S^{\pm} = S^1 \pm iS^2$. This leads to an equivalent representation of the measured operator

$$\mathcal{O}_3 = 2(S_x^1 S_y^1 - S_x^2 S_y^2). \tag{4.31}$$

From this formulation one can see that the process measures the difference between the product of the first components of the spins at the sites x and y and the product of the second components of the spins at the sites x and y. This process conserves the staggered magnetization $\mathcal{M}_s = \sum_{z \in \Lambda} (-1)^{(z_1, z_2)} S_z^3$

$$\left[(S_x^1 S_y^1 - S_x^2 S_y^2), \mathcal{M}_s \right] = 0, \tag{4.32}$$

where x and y are nearest neighbors. The matrix representation of this measurement process is

$$S_x^+ S_y^+ + S_x^- S_y^- = \begin{pmatrix} 0 & 0 & 0 & 1 \\ 0 & 0 & 0 & 0 \\ 0 & 0 & 0 & 0 \\ 1 & 0 & 0 & 0 \end{pmatrix}. \tag{4.33}$$

If the first and second components of the spin are parallel or anti-parallel the measurement outcome is 0. If the first components of the spin are parallel and the second components of the spin are anti-parallel the measurement outcome is +1. With anti-parallel first components and parallel second components the measurement outcome is -1. This leads to three projection operators.

The two eigenstates for the measurement result 0 are

$$EV_1 = |\uparrow\downarrow\rangle, \qquad EV_2 = |\downarrow\uparrow\rangle, \tag{4.34}$$

for the measurement result +1 the eigenstate is

$$EV_3 = \frac{1}{\sqrt{2}}(|\uparrow\uparrow\rangle + |\downarrow\downarrow\rangle), \tag{4.35}$$

and for the measurement result -1 the eigenstate is

$$EV_4 = \frac{1}{\sqrt{2}}(|\uparrow\uparrow\rangle - |\downarrow\downarrow\rangle). \tag{4.36}$$

The projection operators are

$$P_0 = \begin{pmatrix} 0 & 0 & 0 & 0 \\ 0 & 1 & 0 & 0 \\ 0 & 0 & 1 & 0 \\ 0 & 0 & 0 & 0 \end{pmatrix}, P_1 = \begin{pmatrix} \frac{1}{2} & 0 & 0 & \frac{1}{2} \\ 0 & 0 & 0 & 0 \\ 0 & 0 & 0 & 0 \\ \frac{1}{2} & 0 & 0 & \frac{1}{2} \end{pmatrix}, P_{-1} = \frac{1}{2}\begin{pmatrix} \frac{1}{2} & 0 & 0 & -\frac{1}{2} \\ 0 & 0 & 0 & 0 \\ 0 & 0 & 0 & 0 \\ -\frac{1}{2} & 0 & 0 & \frac{1}{2} \end{pmatrix}. \tag{4.37}$$

The elements of the transfer matrix $\tilde{\mathbb{P}} = P_0 \otimes P_0^* + P_1 \otimes P_1^* + P_{-1} \otimes P_{-1}^*$ are written as

$$\begin{aligned} &\langle s_{x,k-1}s_{y,k-1}s'_{x,k-1}s'_{y,k-1}|\,\tilde{\mathbb{P}}\,|s_{x,k-1}s_{y,k-1}s'_{x,k-1}s'_{y,k-1}\rangle \\ &\quad = 4s_{x,k-1}s'_{x,k-1}(s_{x,k-1}s'_{x,k-1} + s_{x,k}s'_{x,k}) \\ &\qquad \cdot\delta_{s_{x,k-1},s_{y,k-1}}\delta_{s_{x,k},s_{y,k}}\delta_{s'_{x,k-1},s'_{y,k-1}}\delta_{s'_{x,k},s'_{y,k}} \\ &\qquad +4s_{x,k-1}s'_{x,k-1}(s_{x,k-1} + s_{x,k})(s'_{x,k-1} + s'_{x,k}) \\ &\qquad \cdot\delta_{s_{x,k-1},-s_{y,k-1}}\delta_{s_{x,k},-s_{y,k}}\delta_{s'_{x,k-1},-s'_{y,k-1}}\delta_{s'_{x,k},-s'_{y,k}}. \end{aligned} \tag{4.38}$$

This matrix can again be simplified because the spin configurations have to be identical on the forward and on the backward contour. The simplified matrix reads

$$\tilde{\mathrm{P}} = \begin{pmatrix} \frac{1}{2} & 0 & 0 & \frac{1}{2} \\ 0 & 1 & 0 & 0 \\ 0 & 0 & 1 & 0 \\ \frac{1}{2} & 0 & 0 & \frac{1}{2} \end{pmatrix} \tag{4.39}$$

This matrix describes the rules for a two-spin interaction on a link.

4.4.4 Meaning of the Measurements in the 1-Basis

The operators for the measurements stay the same when we change the quantization direction from the 3- to the 1-direction but their meaning changes. The measurement of the total spin $\mathcal{O}_1$ is symmetric under the transformation given in equation (3.30) and therefore a basis change does not affect its meaning. The meaning of the second measurement $\mathcal{O}_2$ changes into a measurement of the second components of the spin $S_x^1 S_y^1 \to {S'}_x^2 {S'}_y^2$. To understand the change in the meaning of the third measurement $\mathcal{O}_3$ we take a look at the raising and lowering operator. Its meaning changes as $S^{\pm} = \frac{1}{2}(\sigma_1 \pm i\sigma_2) \to \frac{1}{2}(\sigma'_2 \pm i\sigma'_3) = {S'}^{\pm}$. This induces a change of $S_x^+ S_y^+ + S_x^- S_y^- \to {S'}_x^+ {S'}_y^+ + {S'}_x^- {S'}_y^-$.

4.5 The Lindblad Evolution

In this section, which is based on [14, 15], we want to describe the evolution of a system that is continuously monitored by its environment. To perform a measurement only with a certain probability per unit of time is such a continuous monitoring process. In the previous section we just made sporadic measurements at every time step t_k to evolve the system.

To be able to describe this evolution with a first order differential equation in time we have to impose that the evolution of the system is "Markovian". This means that the characteristic timescale of the environment τ_E, which is the time the environment needs to forget about the information received from the system, needs to be much smaller than the time scale δt of the dynamics we want to observe. Additionally the timescale δt needs to be much smaller than the characteristic time scale of the system τ_S. The evolution of a density matrix ρ in the continuous time limit $\varepsilon \to 0$ is described by the Lindblad equation

$$\begin{aligned} \frac{d\rho(t)}{dt} &= \frac{1}{\varepsilon}\sum_{k,o_k}\left(L_{o_k}\rho(t)L_{o_k}^\dagger - \frac{1}{2}L_{o_k}^\dagger L_{o_k}\rho(t) - \frac{1}{2}\rho(t)L_{o_k}^\dagger L_{o_k}\right) \\ &= \gamma\sum_k\left(\sum_{o_k} P_{o_k}\rho(t)P_{o_k}\right). \end{aligned} \tag{4.40}$$

Here γ is the probability of measurements per unit of time, $\varepsilon = \delta t = t_{k+1} - t_k$ and the operators $L_{o_k} = \sqrt{\varepsilon\gamma}P_{o_k}$ are called Lindblad operators. These operators characterize the real-time evolution and obey the equation

$$(1 - \varepsilon\gamma N)\mathbb{1} + \sum_{k,o_k} L_{o_k}^\dagger L_{o_k} = \mathbb{1}, \tag{4.41}$$

where $t_k \in \{1, ..., N\}$.

The absence of the Hamiltonian in the Lindblad equation comes from the fact that we consider a real-time dynamics that is entirely driven by measurements. Since our loop-cluster algorithm works in discrete time we have to go back from the continuous-time formulation to discretised time. The density matrix at the discrete time step t_{k+1} is fully determined by the previous density matrix at the time step t_k and given by

$$\rho(t_{k+1}) = \rho(t_k) + \varepsilon\dot{\rho}(t_k) = (1 - \varepsilon\gamma)\rho(t_k) + \varepsilon\gamma\sum_{o_k} P_{o_k}\rho(t_k)P_{o_k}. \tag{4.42}$$

Hence we can construct a path integral along the Keldysh contour the same way we already did for the sporadic measurements in section 4.2. For the probability to reach a final state $|f\rangle = |n_N\rangle$ when starting with an initial density matrix irrespective of the intermediate measurement results we get

$$p_{\rho_0,f} = \sum_i p_i \sum_{\substack{n_1,..,n_{N-1} \\ n'_1,..,n'_{N-1}}} \prod_{k=1}^{N} \langle n_{k-1}n'_{k-1}| \left(1 - \varepsilon\gamma\right)\mathbb{1}\otimes\mathbb{1} + \varepsilon\gamma\,\tilde{\mathbb{P}}_k\,|n_k n'_k\rangle\,. \tag{4.43}$$

This expression means that at the time t_k a measurement on the system is performed with the probability $\varepsilon\gamma$ and with the probability $1-\varepsilon\gamma$ nothing happens. Hence for $\varepsilon\gamma = 1$ we get the real-time evolution for a system that is driven by sporadic measurements at every time step t_k.

4.6 Cluster-Rules in RealTime

4.6.1 Cluster Rules for Sporadic Measurements

Measurement of $\mathcal{O}_1$
The weights for the allowed spin configurations are then

$$\begin{aligned}
\begin{matrix}\uparrow\uparrow\\ \uparrow\uparrow\end{matrix} &= 1 = A + C,\\
\begin{matrix}\uparrow\downarrow\\ \uparrow\downarrow\end{matrix} &= \frac{1}{2} = A + B,\\
\begin{matrix}\uparrow\downarrow\\ \downarrow\uparrow\end{matrix} &= \frac{1}{2} = B + C.
\end{aligned} \tag{4.44}$$

We calculate the weights for A, B and C

$$A = \frac{1}{2}, \qquad B = 0, \qquad C = \frac{1}{2}. \tag{4.45}$$

The B breakup vanishes for this measurement process. The probability to choose a certain breakup on a plaquette with given spin configuration is

$$\begin{aligned}
p_{1,A} &= \tfrac{1}{2}, \qquad p_{2,A} = 1,\\
p_{1,C} &= \tfrac{1}{2}, \qquad p_{3,C} = 1.
\end{aligned} \tag{4.46}$$

Measurement of $\mathcal{O}_2$

The allowed spin configurations on a plaquette are then given by

$$\begin{aligned}
\begin{matrix}\uparrow\uparrow\\ \uparrow\uparrow\end{matrix} &= \frac{1}{2} = A + C,\\
\begin{matrix}\uparrow\downarrow\\ \uparrow\downarrow\end{matrix} &= \frac{1}{2} = A + C',\\
\begin{matrix}\uparrow\downarrow\\ \downarrow\uparrow\end{matrix} &= \frac{1}{2} = A' + C,\\
\begin{matrix}\uparrow\uparrow\\ \downarrow\downarrow\end{matrix} &= \frac{1}{2} = A' + C'.
\end{aligned} \tag{4.47}$$

The B breakup does not occur in these cluster rules. However, in addition to the A and C breakup we also have the A' and the C' breakups which connect anti-parallel spins. All the different breakups have the same weight of $1/4$. This leads to the probability of $1/2$ to choose one of the two proposed breakups on all plaquettes.

Measurement of $\mathcal{O}_3$

The allowed spin configurations and their weights are

$$\begin{aligned} \uparrow\uparrow \\ \uparrow\uparrow \end{aligned} = \frac{1}{2} = A, \qquad \begin{aligned} \uparrow\downarrow \\ \uparrow\downarrow \end{aligned} = 1 = A + C', \qquad \begin{aligned} \uparrow\uparrow \\ \downarrow\downarrow \end{aligned} = \frac{1}{2} = C'. \tag{4.48}$$

Solving the system of equations leads to a value of $1/2$ for A and C'. The probabilities to choose a breakup are then given by

$$\begin{aligned} p_{1,A} &= 1, & p_{2,A} &= \frac{1}{2}, \\ p_{4,C'} &= 1, & p_{2,C'} &= \frac{1}{2}. \end{aligned} \tag{4.49}$$

4.6.2 Cluster Rules for Continuous Monitoring

The cluster rules to simulate a system driven by a Lindblad process are different than for a system driven by sporadic measurements.

For all the measurements the possible bonds on a plaquette do not change but probabilities to choose certain bonds do change. For the measurement of the total spin $\mathcal{O}_1$ the probabilities are

$$p_{1,A} = 1 - \frac{\varepsilon\gamma}{2}, \qquad p_{1,C} = \frac{\varepsilon\gamma}{2}, \qquad p_{2,A} = p_{3,C} = 1. \tag{4.50}$$

For the measurement of $\mathcal{O}_2$ the probabilities change to

$$\begin{aligned} p_{1,A} = p_{2,A} &= 1 - \frac{\varepsilon\gamma}{4 - 2\varepsilon\gamma}, \\ p_{1,C} = p_{2,C'} &= \frac{\varepsilon\gamma}{4 - 2\varepsilon\gamma}, \\ p_{3,A'} = p_{3,C} &= p_{4,A'} = p_{4,C'} = \frac{1}{2}. \end{aligned} \tag{4.51}$$

and the probabilities for the measurement of $\mathcal{O}_3$ are

$$p_{1,A} = 1 - \frac{\varepsilon\gamma}{2}, \qquad p_{1,C} = \frac{\varepsilon\gamma}{2}, \qquad p_{2,A} = p_{3,C} = 1. \tag{4.52}$$

4.7 Observables

To observe the measurement driven real-time behavior of the system we measure the different modes of the magnetization at any time step of the evolution. The Fourier modes of the magnetization for a system quantized in the 3-direction and defined on a $L \times L$ square lattice are

$$S(p,t) = \sum_x \exp[i(p_1 x_1 + p_2 x_2)] S_x^3(t), \tag{4.53}$$

where $p = (p_1, p_2)$ is the momentum with $p_i = \frac{2\pi}{L} n_i,\ i \in \{1, 2\}, n_i \in \{1, ..., L\}$ and $x = (x_1, x_2)$ denotes a site in the spacial lattice. $S^3_x(t)$ is the 3-component of the spin at site (x, t).

The mode with $(p_1, p_2) = (0, 0)$ describes the uniform magnetization

$$\mathcal{M}_u(t) = \sum_x S^3_x(t), \tag{4.54}$$

and the (π, π)-mode represents the staggered magnetization

$$\mathcal{M}_s(t) = \sum_x (-1)^{x_1+x_2} S^3_x(t). \tag{4.55}$$

5 Results and Discussion

Based on numerical simulations with a single-cluster algorithm we will discuss the real-time dynamics of quantum spin systems, defined on a 2-dimensional square lattice, which is driven only by measurements. To build the initial density matrix we use the anti-ferromagnetic Heisenberg model, the ferromagnetic Heisenberg model and the XY-model. The observables we use to study the systems are the Fourier modes of the magnetization that are defined in equation (4.53). The dissipative measurement processes we will use to evolve the system are described in section 4.4.

The dynamics of the Fourier modes depends on the symmetries of the chosen measurement process. However the basic dynamics which we observe shows a similar behavior for all three measurement processes. The characteristic order of the initial model is destroyed by the measurement process and all Fourier modes equilibrate to the same value which we call the attractor. Due to the symmetries of the measurement process some modes are conserved and do not equilibrate.

We briefly discuss the results for a system which is driven by a sporadic measurement process. Thereafter we will consider the dynamics of systems that are continuously monitored by the environment which is described by a Kossakowski-Lindblad process. We will then investigate the equilibration times for different measurement processes.

5.1 Sporadic Measurements

A measurement process is called sporadic if at any time-step t_k a measurement is performed with the probability 1. The different Fourier modes of the magnetization equilibrate very fast for the sporadic measurement process. In Figure 9 we illustrate the real-time evolution driven by the measurement process $\mathcal{O}_3 = S_x^+ S_y^+ + S_x^- S_y^-$ for the three different initial density matrices of the Heisenberg anti-ferromagnet, the Heisenberg ferromagnet and the XY-model. The measurement process $\mathcal{O}_3$ conserves the staggered magnetization. Therefore the (π, π)-mode of the magnetization, which corresponds to the staggered magnetization, does not equilibrate. All the other Fourier modes fall down onto the same attractor A. In Figure 9a we do not see the (π, π)-mode since it is at a very high value and conserved over time. In one time-step $\Delta t = 4\Delta\tau$ a sequence of four measurements is performed.

5.2 Continuous Monitoring

The continuous measurement processes which we study in detail perform measurements on the system with a probability γ per unit time. The equilibration procedure for a continuous measurement process is much smoother than for sporadic measurements. In the following subsections we will discuss the real-time dynamics for the Heisenberg anti-ferromagnet, the Heisenberg ferromagnet and the XY-model initial density matrix driven by the measurement processes

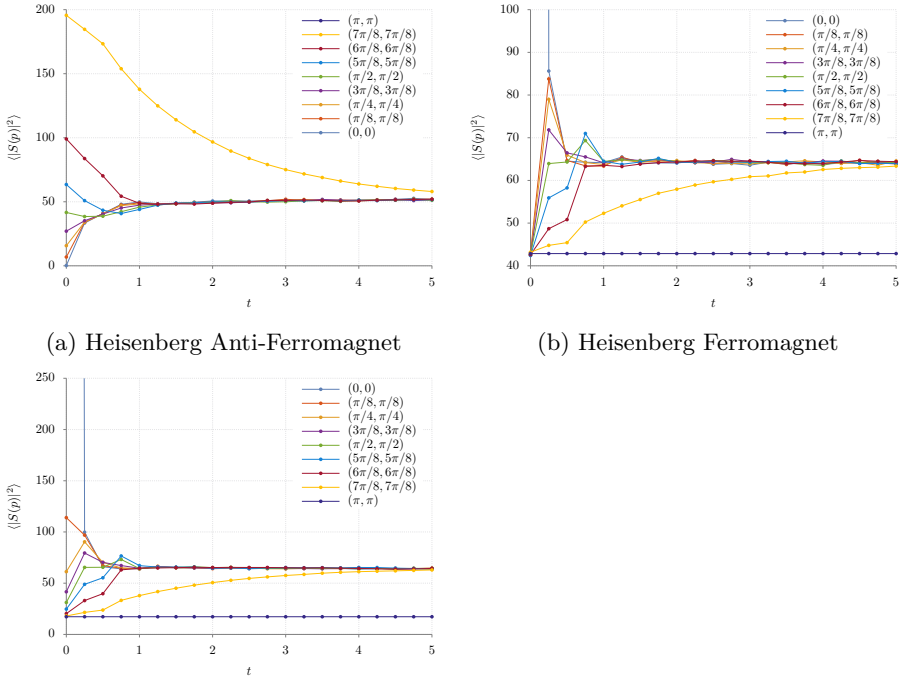

(a) Heisenberg Anti-Ferromagnet

(b) Heisenberg Ferromagnet

(c) XY-Model

Figure 9: Examples for a sporadic measurement process driven by the measurement $\mathcal{O}_3$. The parameters used for the simulation are: $4N_t = 512$, $L = 16$, $\beta J = 40$ and $\varepsilon\gamma = 1$.

$\mathcal{O}_1 = (\vec{S}_x + \vec{S}_y)^2$ and $\mathcal{O}_3 = S_x^+ S_y^+ + S_x^- S_y^-$ and compare it to the dynamics driven by $\mathcal{O}_2 = S_x^1 S_y^1$.

5.2.1 Heisenberg Anti-Ferromagnet Initial Density Matrix

In the anti-ferromagnetic Heisenberg model the most favored configuration of the spins is the staggered configuration. The staggered magnetization is also the order parameter of the system. It is maximal at the temperature $T = 0$ where the system reaches the highest possible order. In contrast to classical systems a quantum system can not reach a perfect Néel order since there still occur quantum fluctuations at zero temperature. Therefore the staggered magnetization is very high at low temperatures while the uniform magnetization vanishes. In Figure 10 we illustrate the evolution of a Heisenberg anti-ferromagnet initial density matrix driven by the measurement of the total spin $\mathcal{O}_1$. This process conserves the $(0, 0)$-mode of the magnetization which corresponds to the uniform magnetization. The closer the modes are to the conserved $(0, 0)$-mode the slower they equilibrate. As one can see in the logarithmic plot of Figure 10 the

(π, π)-mode starts from a very high value and equilibrates faster than all the other modes. Figure 11 shows the dynamics of the Fourier modes driven by the measurement process $\mathcal{O}_3$. Here we can also observe the slow equilibration of the modes close to the conserved (π, π)-mode.

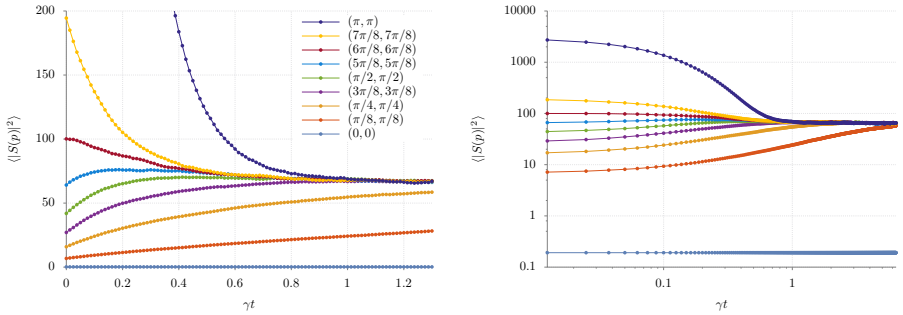

Figure 10: Real-time evolution of the Fourier modes for a Heisenberg anti-ferromagnetic initial density matrix driven by the measurement process $\mathcal{O}_1$. The errors are of the order of the point size and the lines are not a fit but to guide the eye. The parameters used for the simulation are: $4N_t = 512$, $L = 16$, $\beta J = 40$ and $\varepsilon\gamma = 0.05$. *Left*: Linear plot for a short time interval. *Right*: Logarithmic plot for a longer time interval. It also includes the initial value of the staggered magnetization.

5.2.2 Heisenberg Ferromagnet Initial Density Matrix

The order parameter for the Heisenberg ferromagnet is the uniform magnetization or the $(0, 0)$-mode. For low temperatures the uniform magnetization is very high and the other modes have almost the same value close to zero. In Figure 12 we show the real-time evolution of a ferromagnetic initial density matrix driven by the measurement process $\mathcal{O}_1$. The different modes are almost conserved since the $(0, 0)$-mode is conserved and all the other modes almost lie on the attractor from the beginning. In Figure 13 we illustrate the evolution from a ferromagnetic initial density matrix driven by the measurement process $\mathcal{O}_3$. The $(0, 0)$-mode is not conserved any more and it falls down to the attractor very quickly. Besides the (π, π)-mode, which is conserved for this process, all the other modes are pulled up to the attractor from below.

5.2.3 XY-Model Initial Density Matrix

To study the XY-model we changed from the 3-basis to the 1-basis. In this basis the order parameter of the system is the uniform magnetization or the $(0, 0)$-mode. In Figure 14 we illustrate the dynamics driven by the measurement process $\mathcal{O}_1$. It looks similar to the dynamics of the Heisenberg anti-ferromagnetic initial density matrix driven by the measurement process $\mathcal{O}_3$. While the dynamics in Figure 15 is driven by the measurement process $\mathcal{O}_3$ it is reminiscent of

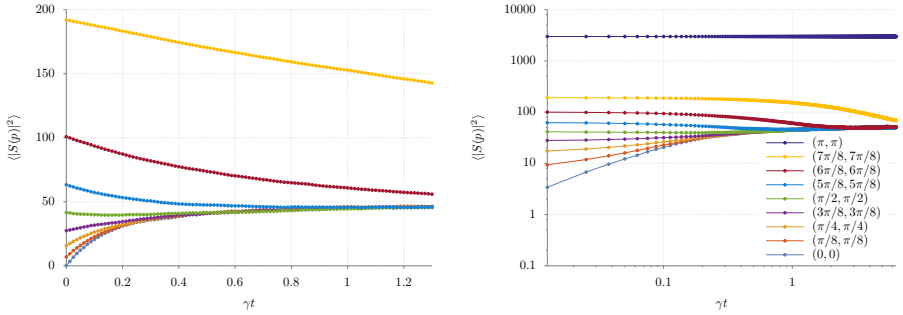

Figure 11: Real-time evolution of the Fourier modes for a Heisenberg anti-ferromagnetic initial density matrix driven by the measurement process $\mathcal{O}_3$. The errors are again of the order of the point size and the lines are there to guide the eye. The parameters are the same as in Figure 10. *Left*: Linear plot for a short time interval. *Right*: Logarithmic plot for a longer time interval. It also includes the initial value of the staggered magnetization.

the dynamics of the Heisenberg anti-ferromagnetic initial density matrix driven by $\mathcal{O}_1$.

5.2.4 The Measurement Process $\mathcal{O}_2$

Since the measurement process $\mathcal{O}_2 = S^1_x S^1_y$ does not conserve any of the Fourier modes there are no slowly equilibrating modes as for the measurement processes $\mathcal{O}_1$ and $\mathcal{O}_3$. All modes fall on the attractor very quickly as one can see in Figure 16.

5.3 Equilibration Times

For the analysis of the equilibration times we assume that the different Fourier modes equilibrate independent of each other. This is not exactly true as we will see later.

In the previous subsection we have seen that the different modes approach the attractor exponentially with an equilibration time $\tau(p)$. For the Heisenberg anti-ferromagnet initial density matrix we fit a number of Fourier modes close to the $(0,0)$- and the (π,π)-mode according to

$$\langle |S(p)|^2 \rangle \to A(p) + B(p) \exp\Big(- \frac{t}{\tau(p)} \Big). \tag{5.1}$$

In Figure 17 we show the inverse equilibration time depending on the momentum for the three measurement processes $\mathcal{O}_1$, $\mathcal{O}_2$ and $\mathcal{O}_3$ for the Heisenberg anti-ferromagnetic initial density matrix. The inverse equilibration time for the measurement process $\mathcal{O}_1$ behaves like

$$\frac{1}{\gamma \tau(p)} = C|ap|^r, \quad C = 1.29(4),\ r = 1.9(1), \tag{5.2}$$

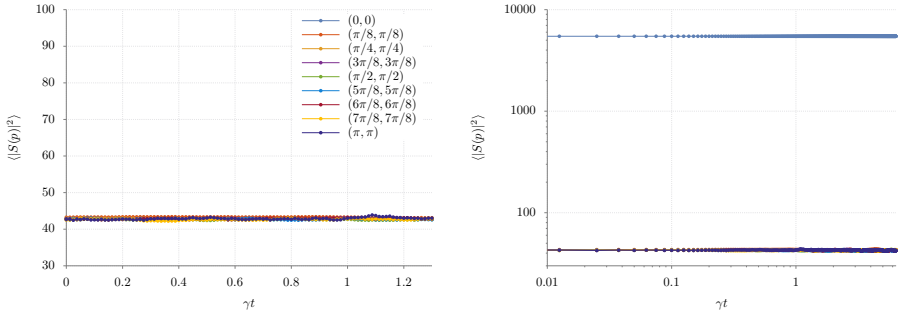

Figure 12: Real-time evolution of the Fourier modes for a Heisenberg ferromagnetic initial density matrix driven by the measurement process $\mathcal{O}_1$. The errors are again of the order of the point size and the lines are there to guide the eye. The parameters are the same as in Figure 10. *Left*: Linear plot for a short time interval. *Right*: Logarithmic plot for a longer time interval. It also includes the initial value of the uniform magnetization.

for small momenta p. This result is in good agreement with the values obtained in [12] and [13]. For the measurement process $\mathcal{O}_3$ at high momenta the inverse equilibration time corresponds to

$$\frac{1}{\gamma\tau(p)} = C|ap|^r, \quad C = 1.19(2),\ r = 2.1(1), \tag{5.3}$$

Actually it is more tricky to fit the Fourier modes. As we see in Figure 13 the modes from below tend to overshoot and then approach the attractor from above. This means that the modes can not be fitted by a simple exponential model but all the modes would need to be fitted simultaneously. This occurs because the Fourier modes can not evolve independently from each other. Their behavior is restricted by the fact that the sum over all modes of the squared magnetization is conserved over time

$$\sum_p \langle |S(p)|^2 \rangle = const. \tag{5.4}$$

This means that we can calculate the exact attractor A, that all non-conserved modes equilibrate to, which is indicated in Figure 13 by a straight line. For a detailed analysis of the behavior of the Fourier modes see [13].

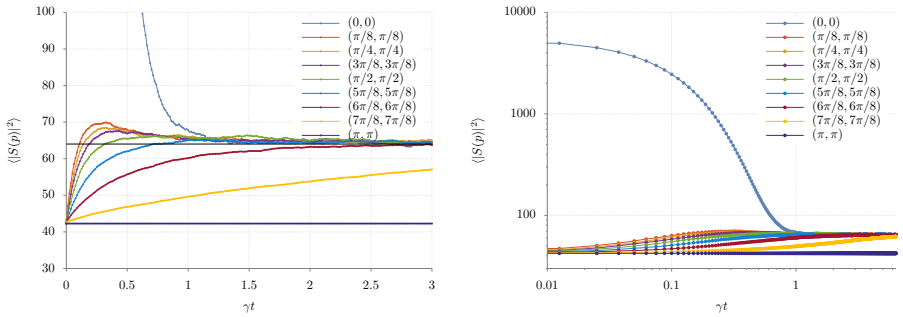

Figure 13: Real-time evolution of the Fourier modes for a Heisenberg ferromagnetic initial density matrix driven by the measurement process $\mathcal{O}_3$. The errors are again of the order of the point size and the lines are there to guide the eye. The parameters are the same as in Figure 10. *Left*: Linear plot for a short time interval supplemented with the analytically calculated attractor (black line). *Right*: Logarithmic plot for a longer time interval. It also includes the initial value of the uniform magnetization.

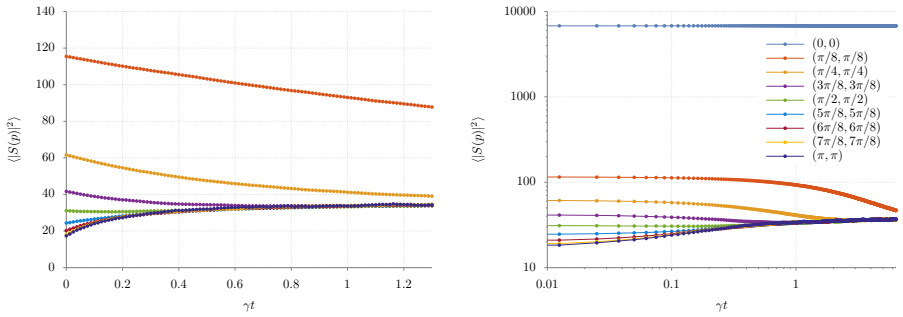

Figure 14: Real-time evolution of the Fourier modes for an XY-model initial density matrix driven by the measurement process $\mathcal{O}_1$. The errors are again of the order of the point size and the lines are there to guide the eye. The parameters are the same as in Figure 10. *Left*: Linear plot for a short time interval. *Right*: Logarithmic plot for a longer time interval. It also includes the initial value of the uniform magnetization.

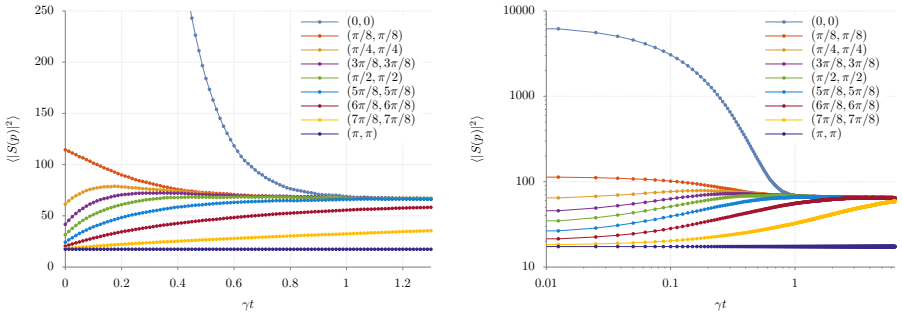

Figure 15: Real-time evolution of the Fourier modes for an XY-model initial density matrix driven by the measurement process $\mathcal{O}_3$. The errors are again of the order of the point size and the lines are there to guide the eye. The parameters are the same as in Figure 10. *Left*: Linear plot for a short time interval. *Right*: Logarithmic plot for a longer time interval. It also includes the initial value of the uniform magnetization.

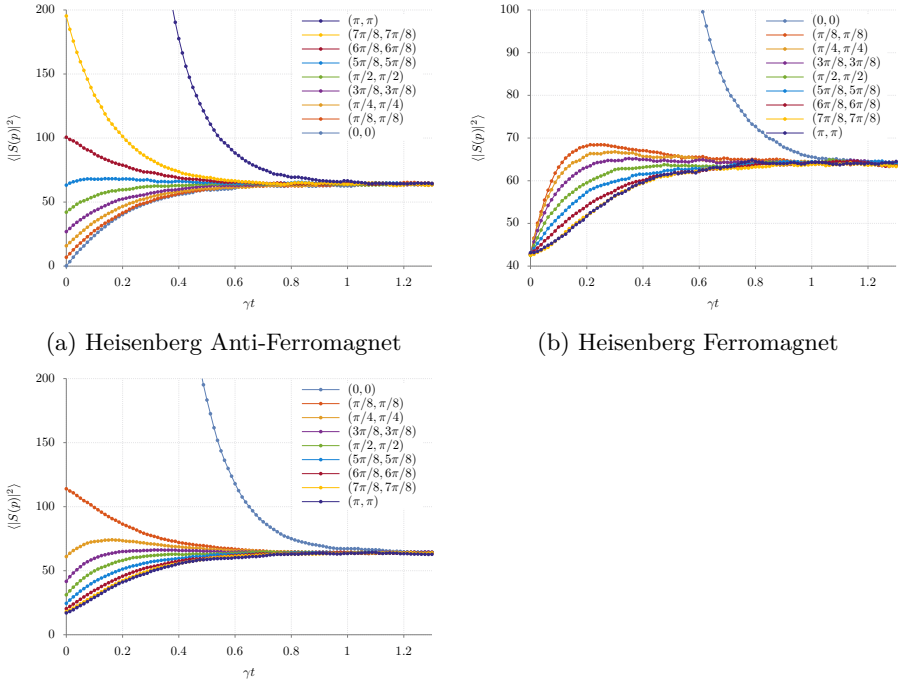

(a) Heisenberg Anti-Ferromagnet

(b) Heisenberg Ferromagnet

(c) XY-Model

Figure 16: Dynamics of the Fourier modes driven by the measurement process $\mathcal{O}_2$ for the Heisenberg anti-ferromagnetic, the Heisenberg ferromagnetic and the XY-model initial density matrix. The errors are again of the order of the point size and the lines are there to guide the eye. The parameters are the same as in Figure 10.

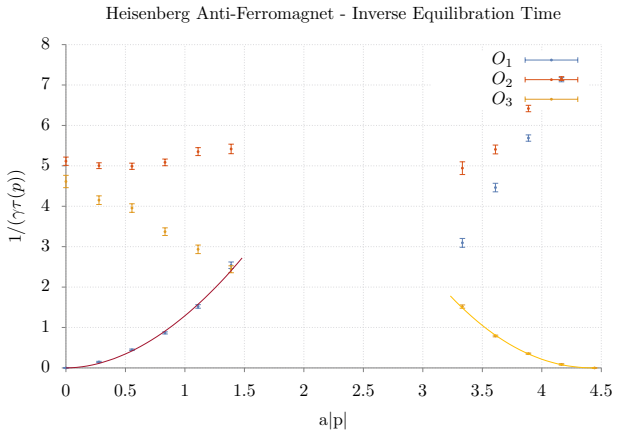

Figure 17: Inverse equilibration time for the three different measurement processes with a Heisenberg anti-ferromagnet initial density matrix. The parameters used for the simulation are: $4N_t = 512$, $L = 32$, $\beta J = 40$ and $\varepsilon\gamma = 0.05$.

6 Conclusion and Outlook

We have simulated different quantum spin 1/2 systems on a 2-dimensional square lattice at low temperature. The systems are coupled to an environment through a dissipative measurement processes and the Hamiltonian is set to zero which means that the dynamics of the system is entirely driven by measurements. The evolution of the system is either driven by sporadic measurements or by a continuous monitoring through the environment described by the Kossakowski-Lindblad equation.

The system was simulated with a loop-cluster algorithm for which we derived the real-time cluster-rules. This algorithm could easily be applied to higher dimensional quantum spin systems. From the simulation we see that the initial order of the system is destroyed by the measurement process and the system is driven to a new equilibrium state. The initial state had long-range correlations whereas the new equilibrium state has only short range correlations. Depending on the symmetries of the measurement process some of the Fourier modes equilibrate slower or not at all. Further investigations on the inverse equilibration times of the Fourier modes show a quadratic momentum dependence. The approach towards the attractor can therefore be viewed as a diffusion process of the conserved quantity.

This work is to be considered as a first step on the way to the real-time simulation of quantum systems with a non trivial Hamiltonian. While we set the Hamiltonian to zero and couple the system to the environment it behaves much less quantum and we are able to get rid of the sign problem. The big challenge is to re-include the full Hamiltonian into these calculations and to combine the coupling to the environment with the intrinsic dynamics of the system. It is interesting to investigate whether the meron cluster algorithm could solve the sign problem caused by non-trivial Hamiltonians. Another project is to adapt this formalism to fermionic systems.

Acknowledgement

I thank Prof. Dr. Uwe-Jens Wiese for the support during the writing of this thesis. He included us into discussion with his research group and was always a source for new motivation. Further I thank Dr. Debasish Banerjee and Dr. Florian Hebenstreit for the detailed explanations and for answering all sorts of questions. Finally I thank Manes Hornung for the collaboration, for illuminating discussions and for useful hints to further literature.

A Data Analysis

The loop-cluster algorithm has very small autocorrelation times. Nevertheless are the data correlated and we need to analyze them with appropriate statistical methods. First we want to calculate the error of the mean over a set of correlated data. Then we explain how to determine a non-linear function of averages. This appendix is based on [17].

A.1 Average and Error

Suppose we have a sample of N independent data points $x_i,\ i = 1, ..., N$ generated by a simulation. These data points are governed by the hidden distribution $P(x)$ which is normalized to one

$$\int_{-\infty}^{\infty} P(x)\mathrm{d}x = 1. \tag{A.1}$$

The exact mean μ and the variance σ^2 of the distribution are given by

$$\mu = \langle x \rangle, \qquad \sigma^2 = \langle (x - \langle x \rangle)^2 \rangle = \langle x^2 \rangle - \langle x \rangle^2, \tag{A.2}$$

where $\langle x \rangle$ and $\langle x^2 \rangle$ are the first and the second moments of the distribution $P(x)$. The n-th moment of the distribution is defined as

$$\langle x^n \rangle = \int_{-\infty}^{\infty} x^n P(x)\mathrm{d}x. \tag{A.3}$$

In general we do not know this hidden distribution $P(x)$. Therefore we are not able to calculate the exact values of μ and σ^2 but we can calculate the sample mean $\bar{x}$ and the sample variance s^2 according to

$$\bar{x} = \frac{1}{N}\sum_{i=1}^{N} x_i, \qquad s^2 = \frac{1}{N}\sum_{i=1}^{N} (x_i - \bar{x})^2. \tag{A.4}$$

In the limit of infinitely many measurements N the sample mean $\bar{x}$ converges to the real mean $\mu = \langle x \rangle$. We are now interested in the error of the sample mean

$$\begin{aligned}
\sigma_{\bar{x}}^2 &= \langle (\bar{x} - \mu)^2 \rangle \\
&= \Big\langle \Big(\frac{1}{N}\sum_{i=1}^{N} x_i - \mu \Big)^2 \Big\rangle \\
&= \frac{1}{N^2} \Big\langle \sum_{i=1}^{N} (x_i - \mu)^2 + \sum_{i \neq j; i,j=1}^{N} (x_i - \mu)(x_j - \mu) \Big\rangle \\
&= \frac{1}{N^2} \Big\langle \sum_{i=1}^{N} (x_i - \mu)^2 \Big\rangle \\
&= \frac{\sigma^2}{N}.
\end{aligned} \tag{A.5}$$

The second term in the third line of equation (A.5) is zero since we assume the data to be statistically independent which means that $\langle x_i x_j \rangle = \langle x_i \rangle \langle x_j \rangle$ for $i \neq j$. The quantity σ^2 in equation (A.5) is the exact variance which we are not able to calculate. However, we do know the relation between $\langle s^2 \rangle$ and σ^2

$$\langle s^2 \rangle = \frac{N-1}{N} \sigma^2. \tag{A.6}$$

The best estimate for σ^2 is given by $\frac{N}{N-1} s^2$. The exact mean is written as

$$\mu = \bar{x} \pm \sigma_{\bar{x}}, \qquad \text{with} \quad \sigma_{\bar{x}} = \frac{s}{\sqrt{N-1}}. \tag{A.7}$$

The data generated by a simulation are usually not independent. Performing a binning on the data is an efficient way to get less correlated data. We define b as the bin size and $N/b = N_B$ is the number of bins which corresponds to the new number of data points. The bin size b has to be chosen in a way that N is divisible by b without remainder. It also needs to be big enough in order to obtain a set of independent data points but otherwise needs to be small enough to create sufficiently bins to get a good estimate of $\sigma_{\bar{x}}$. The binned data points are given by

$$x_{b_i} = \frac{1}{b} \sum_{j=(i-1)b+1}^{ib} x_j, \quad i = 1, 2, ..., N_B. \tag{A.8}$$

With these new less correlated data points we can calculate the mean and its error with the formulas derived above.

A.2 Jackknife

We want to calculate the estimate and the error of a function of averages $f(\mu_1, ..., \mu_N)$. Here we restrict ourselves to only two variables since the generalization to N variables is obvious. The quantity $f(\bar{x}, \bar{y})$ is a sample-based estimate of the function $f(\mu_x, \mu_y)$. If the function is non-linear we have to notice that this estimate has a bias of order $\mathcal{O}(1/N)$. To calculate the error of such a non-linear function of averages in a traditional way is rather complicated since one has to perform an error propagation after Gauss. A comfortable way to automate the calculation of the error is to re-sample the data with the Jackknife method. This re-sampling method additionally removes the leading order contribution to the bias. Although the bias was only a small effect of order $\mathcal{O}(1/N)$ in contrast to the statistical error which is of order $\mathcal{O}(1/\sqrt{N})$.

The i-th Jackknife estimate is defined as the average over all the data in the sample except the data point x_i

$$x_i^J = \frac{1}{N-1} \sum_{\substack{j=1 \\ j \neq i}}^{N} x_j, \quad i = 1, ..., N. \tag{A.9}$$

The Jackknife estimate for $f(\mu_x, \mu_y)$ is then defined as

$$\overline{f^J} = \frac{1}{N}\sum_{i=1}^{N} f_i^J, \qquad \text{with} \quad f_i^J = f(x_i^J, y_i^J). \tag{A.10}$$

The variance of the Jackknife estimate is defined as

$$s_{f^J}^2 = \overline{(f^J)^2} - (\overline{f^J})^2 \qquad \text{with} \quad \overline{(f^J)^2} = \frac{1}{N}\sum_{i=1}^{N}(f_i^J)^2. \tag{A.11}$$

The best estimate for the error σ_f is $\sqrt{N-1}s_{f^J}$. Hence

$$f(\mu_x, \mu_y) = \overline{f^J} \pm \sqrt{N-1}s_{f^J}. \tag{A.12}$$

Another method to automatically calculate the error of a function of averages without having to keep track of all the variances, covariances and partial derivatives from the Gaussian error propagation is the Bootstrap method. This method is similar to the Jackknife method. The difference is that the N_{boot} new data sets are built by randomly picking N data points out of the original data set where the probability to pick a point is always $1/N$. The same point therefore can be picked up several times for one data set. For this method the calculation of the mean and the standard deviation stays the same. The mean is denoted by $\overline{f^B}$ and the standard deviation is denoted by s_{f^B}. For the error we get a new formula. Hence

$$f(\mu_x, \mu_y) = \overline{f^B} \pm \sqrt{\frac{N}{N-1}}s_{f^B}. \tag{A.13}$$

For the calculation of the fit in section 5.3 we used the Jackknife re-sampling method.

B Units

The SI unit of the spin is the joule-second [Js] which is also the unit of the classical angular momentum. However we can express the spin as a multiple of the reduced Planck constant $\hbar$ which also has the dimension of an action. Since we work in natural units with $c = \hbar = k_B = 1$ the spin and hence also the magnetization are unit-less quantities. Length and time are given in units of inverse energy.

References

[1] S. R. White, *Density matrix formulation for quantum renormalization groups*, Phys. Rev. Lett. **69** (1992), 2863

[2] U. Schollwöck, *The density-matrix renormalization group*, Rev. Modern Phys. **77** (2005), 259

[3] A. E. Feiguin and S. R. White, *Time-step targeting methods for real-time dynamics using the density matrix renormalization group*, Phys. Rev. B **72** (2005) (2), 020404

[4] R. P. Feynman, *Simulating physics with computers*, Internat. J. Theoret. Phys. **21** (1982), 467

[5] A. Kossakowski, *On quantum statistical mechanics of non-Hamiltonian systems*, Rep. Math. Phys. **3** (1972), 247

[6] G. Lindblad, *On the generators of quantum dynamical semigroups*, Comm. Math. Phys. **48** (1976), 119

[7] B. B. Beard and U.-J. Wiese, *Simulations of discrete quantum systems in continuous Euclidean time*, Phys. Rev. Lett. **77** (1996), 5130

[8] *Louis Néel - Facts*, `http://www.nobelprize.org/nobel_prizes/physics/laureates/1970/neel-facts.html`, accessed: 22 Mar 2015

[9] H. G. Evertz, *The loop algorithm*, Adv. Phys. **52** (2003), 1

[10] R. Brower, S. Chandrasekharan and U.-J. Wiese, *Green's functions from quantum cluster algorithms*, Phys A **261** (1998), 520

[11] U.-J. Wiese and H.-P. Ying, *A determination of the low energy parameters of the 2-d Heisenberg antiferromagnet*, Z. Phys. B **93** (1994), 147

[12] D. Banerjee, F.-J. Jiang, M. Kon and U.-J. Wiese, *Real-time simulation of large open quantum spin systems driven by dissipation*, Phys. Rev. B **90** (2014), 241104

[13] F. Hebenstreit, D. Banerjee, M. Hornung, F.-J. Jiang, F. Schranz and U.-J. Wiese, *Real-time dynamics of open quantum spin systems driven by dissipative processes*, ArXiv e-prints (2015)

[14] J. Preskill, *Lecture notes for physics 229: Quantum information and computation* (1998)

[15] A. J. Fisher *et al.*, *Graduate course on open quantum systems*

[16] R. van Leeuwen, N. Dahlen, G. Stefanucci, C.-O. Almbladh and U. von Barth, *Introduction to the Keldysh formalism*, Lecture Notes in Phys. **706** (2006), 33

[17] P. Young, *Everything you wanted to know about Data Analysis and Fitting but were afraid to ask*, ArXiv e-prints (2014)